

V. CROSS SECTIONS

V.A. Proton and Deuteron Cross Sections

In the approximation of single photon exchange, the radiatively corrected cross sections are linear in the two structure functions W_1 and W_2 , according to equation (I.1). We exploit this fact in presenting the e-p and e-d cross section data graphically. The data for vW_2^P and vW_2^d are plotted versus W in Figures (9 - 16). They were extracted from the measured cross sections assuming $R_p = R_d = 0.18$ in equation (I.5). The solid lines represent global fits to vW_2^P and vW_2^d that will be discussed in section V.C. As is evident from figures (9 - 16), most of the data of experiment B and some of the 18° data of experiment A exist as "fine-mesh" cross sections computed, as discussed earlier, using the angle and momentum information from the two hodoscopes. This fine resolution was indispensable in the resonance region and also at small $\omega \leq 2$ where the magnitude of the deuteron binding correction varies sharply over the spectrometer acceptance. These fine-mesh data were accordingly used in the study of the resonances and in the extraction of the neutron cross sections, as described in section VD. On the other hand, studies of the structure functions and R in the deep inelastic region did not require such fine resolution. For these studies, the fine-mesh data for $W \geq 1.8$ GeV were combined into statistically more precise cross sections

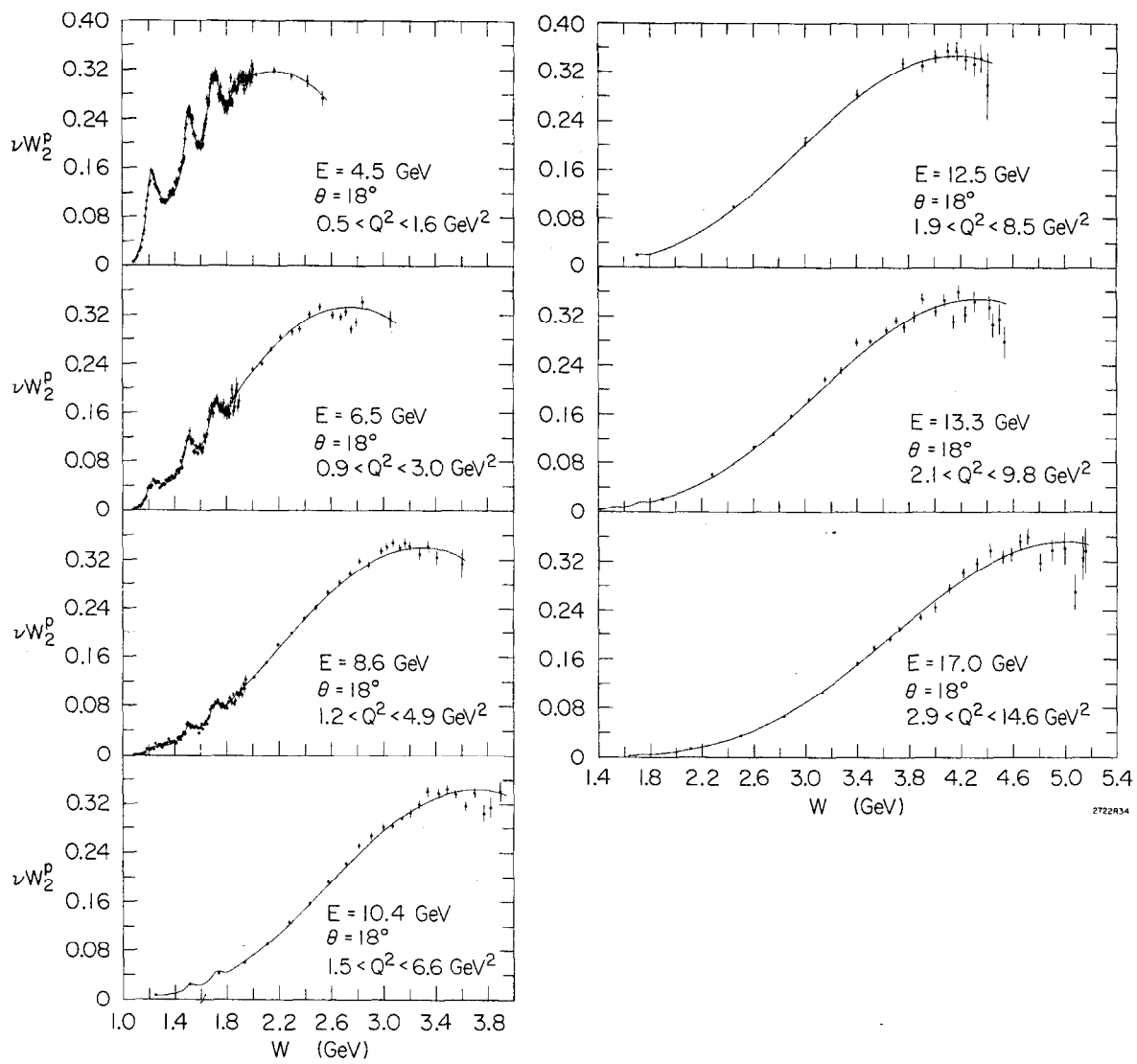


Fig. 9. The quantity νW_2^p extracted from inelastic e - p cross sections measured at 18° in experiment A assuming $R_p = 0.18$.

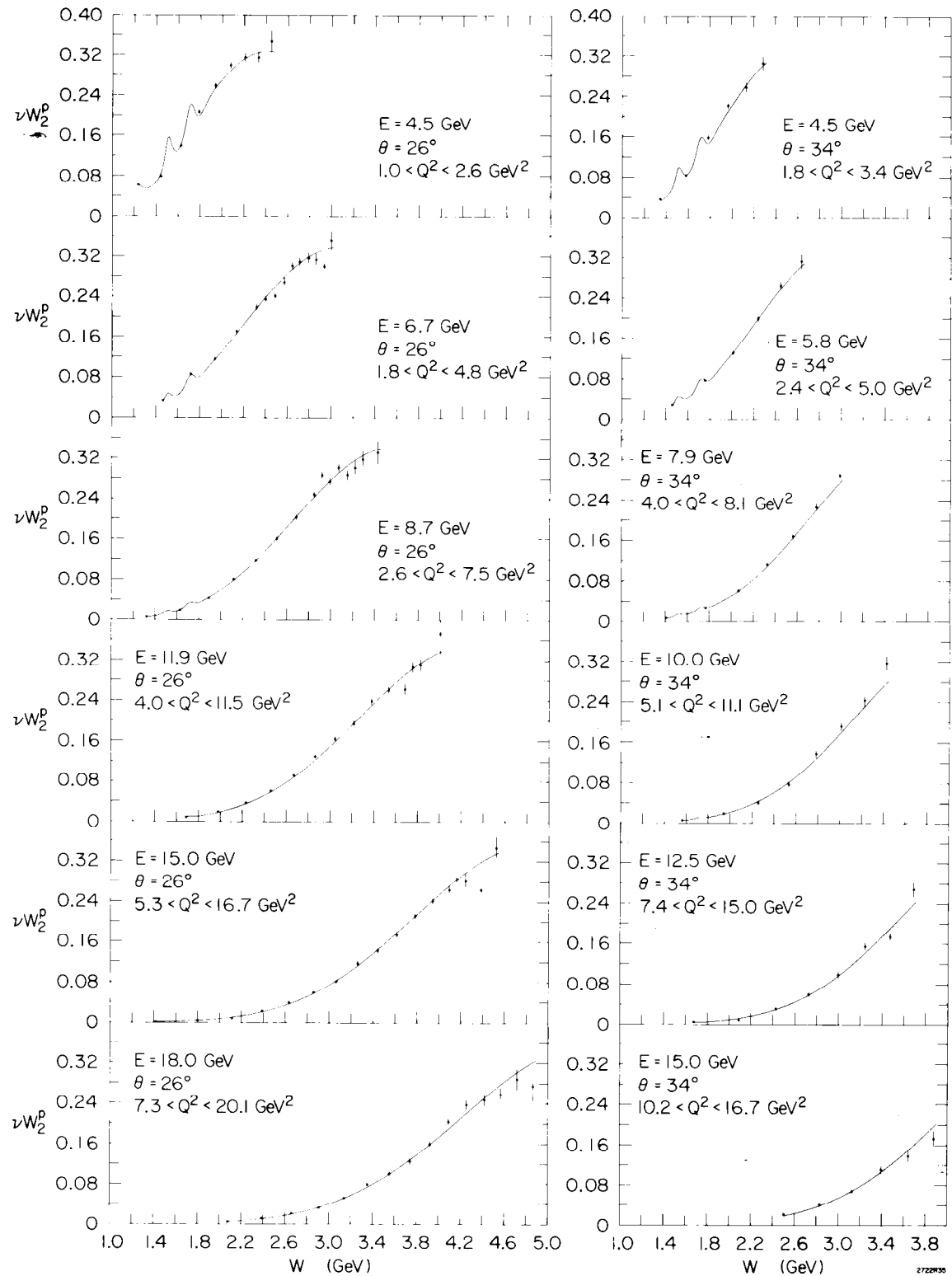


Fig. 10. The quantity νW_2^P extracted from inelastic $e - p$ cross sections measured at 26° and 34° in experiment A assuming $R_p = 0.18$.

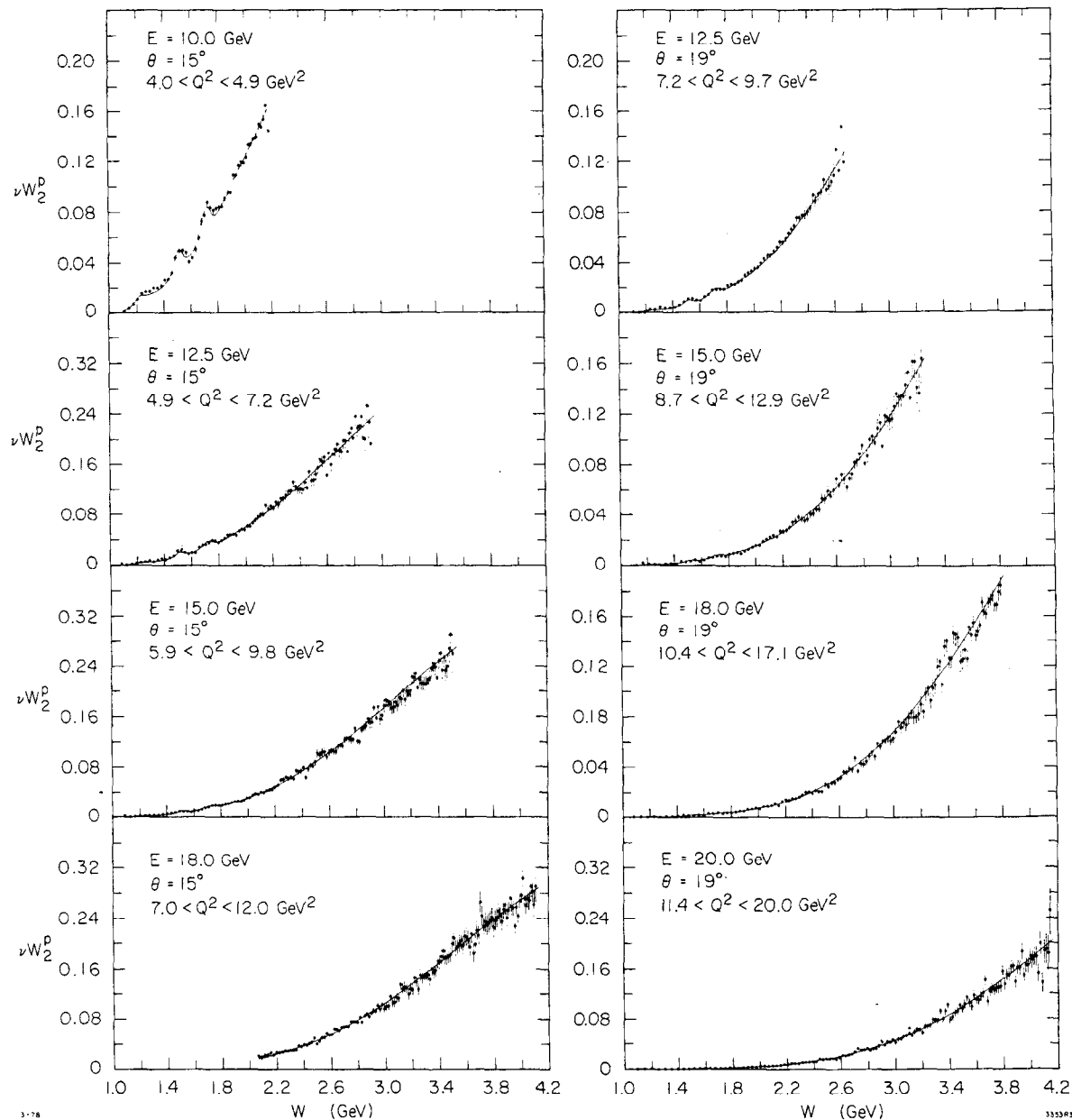


Fig. 11. The quantity νW_2^p extracted from inelastic $e - p$ cross sections measured at 15° and 19° in experiment B assuming $R_p = 0.18$.

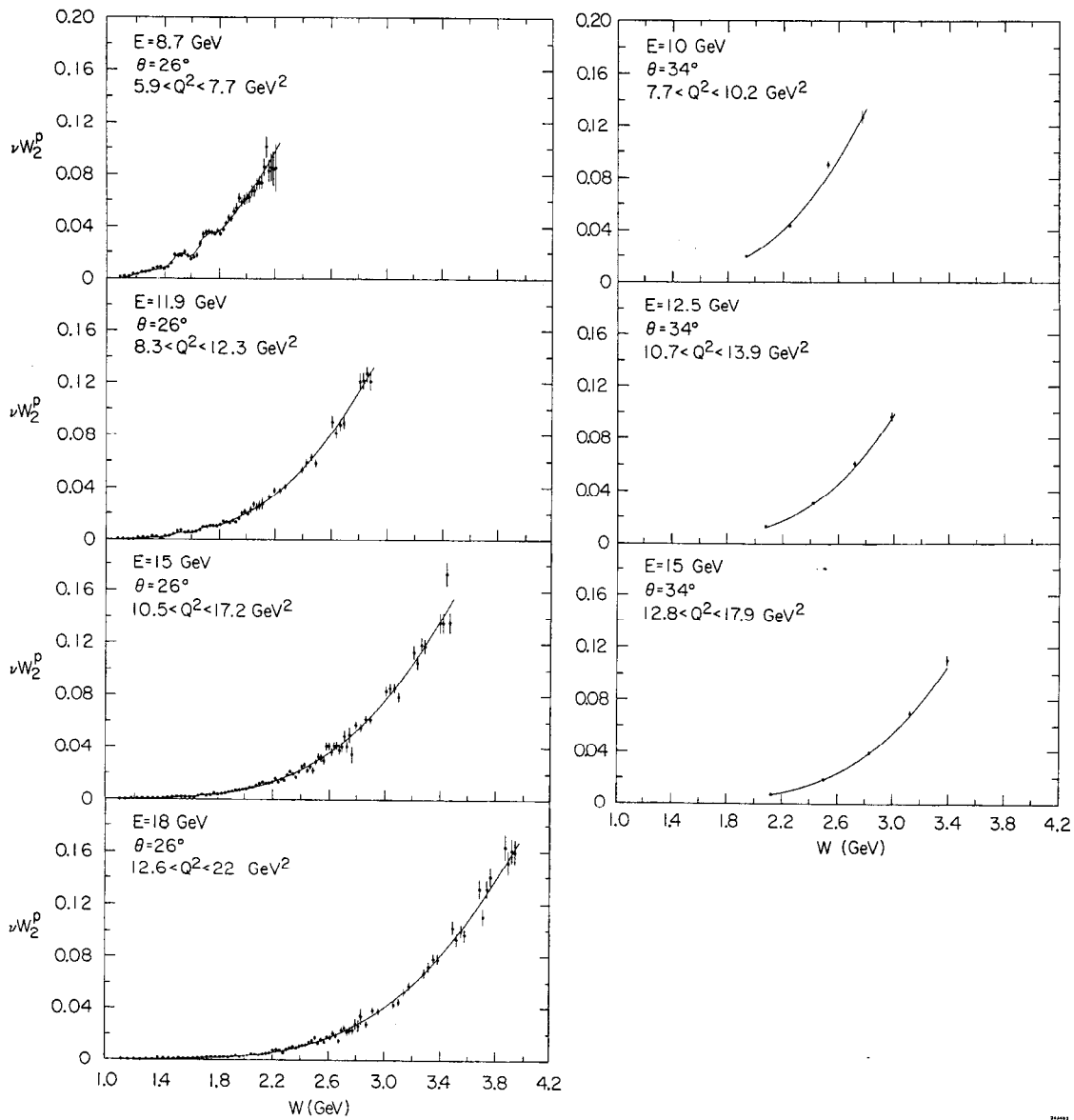


Fig. 12. The quantity νW_2^P extracted from inelastic $e - p$ cross sections measured at 26° and 34° in experiment B assuming $R_p = 0.18$.

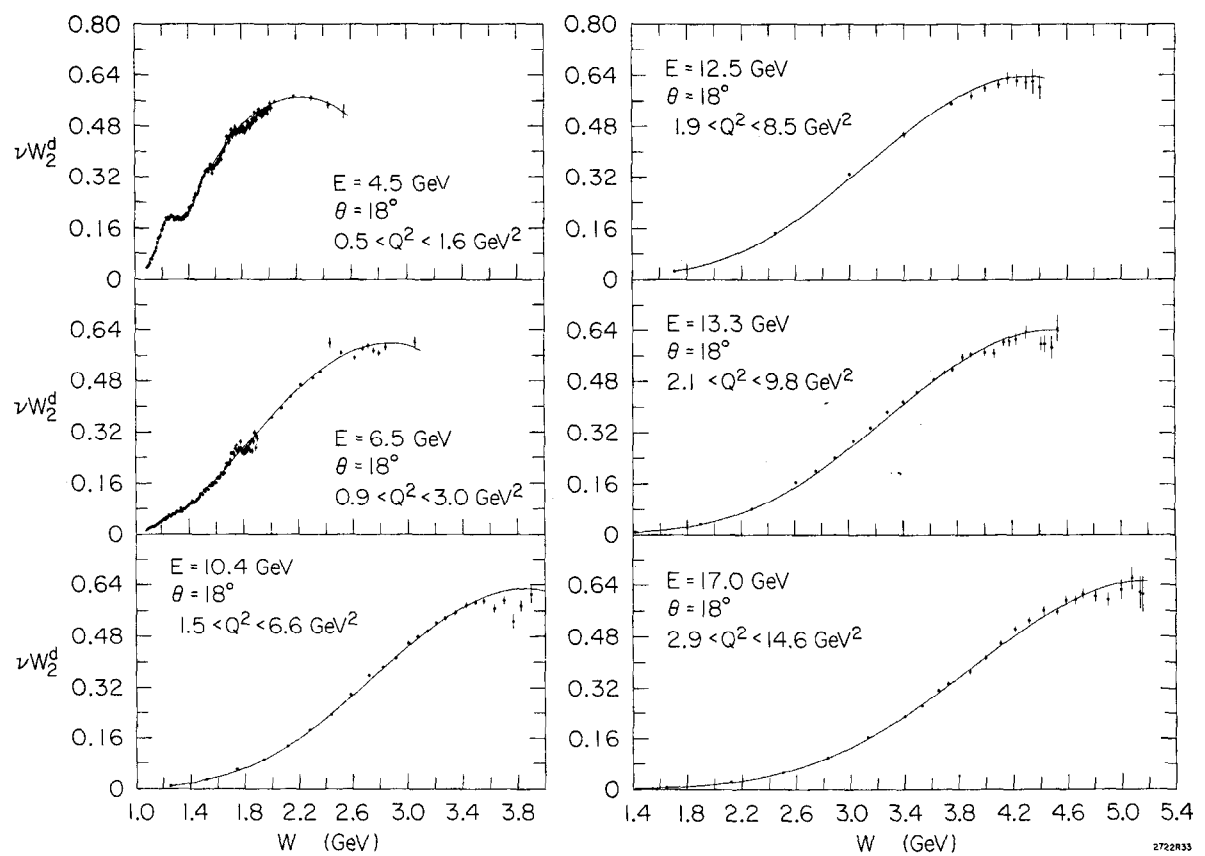


Fig. 13. The quantity νW_2^d extracted from inelastic $e - d$ cross sections measured at 18° in experiment A assuming $R_d = 0.18$.

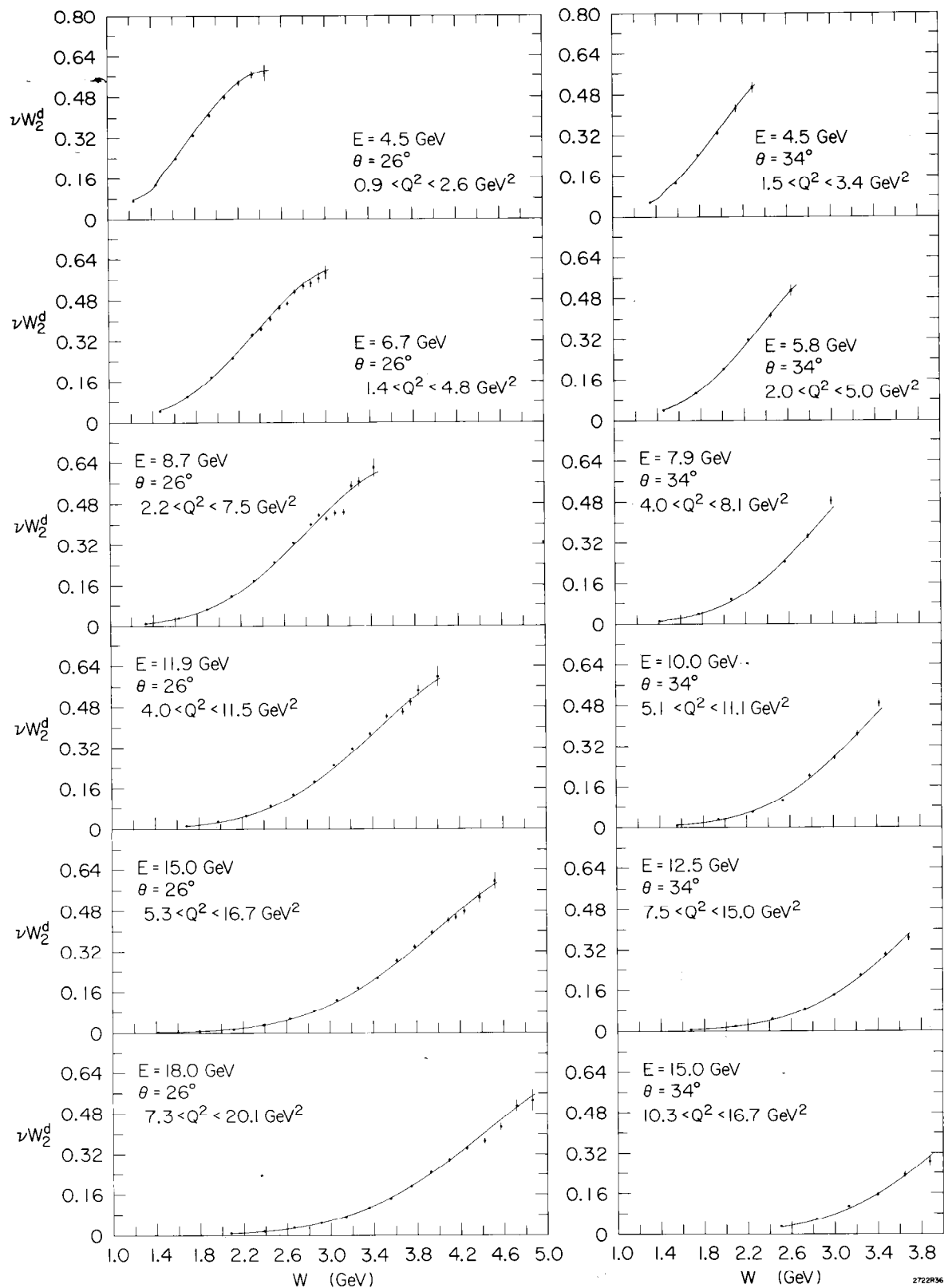


Fig. 14. The quantity νW_2^d extracted from inelastic $e - d$ cross sections measured at 26° and 34° in experiment A assuming $R_d = 0.18$.

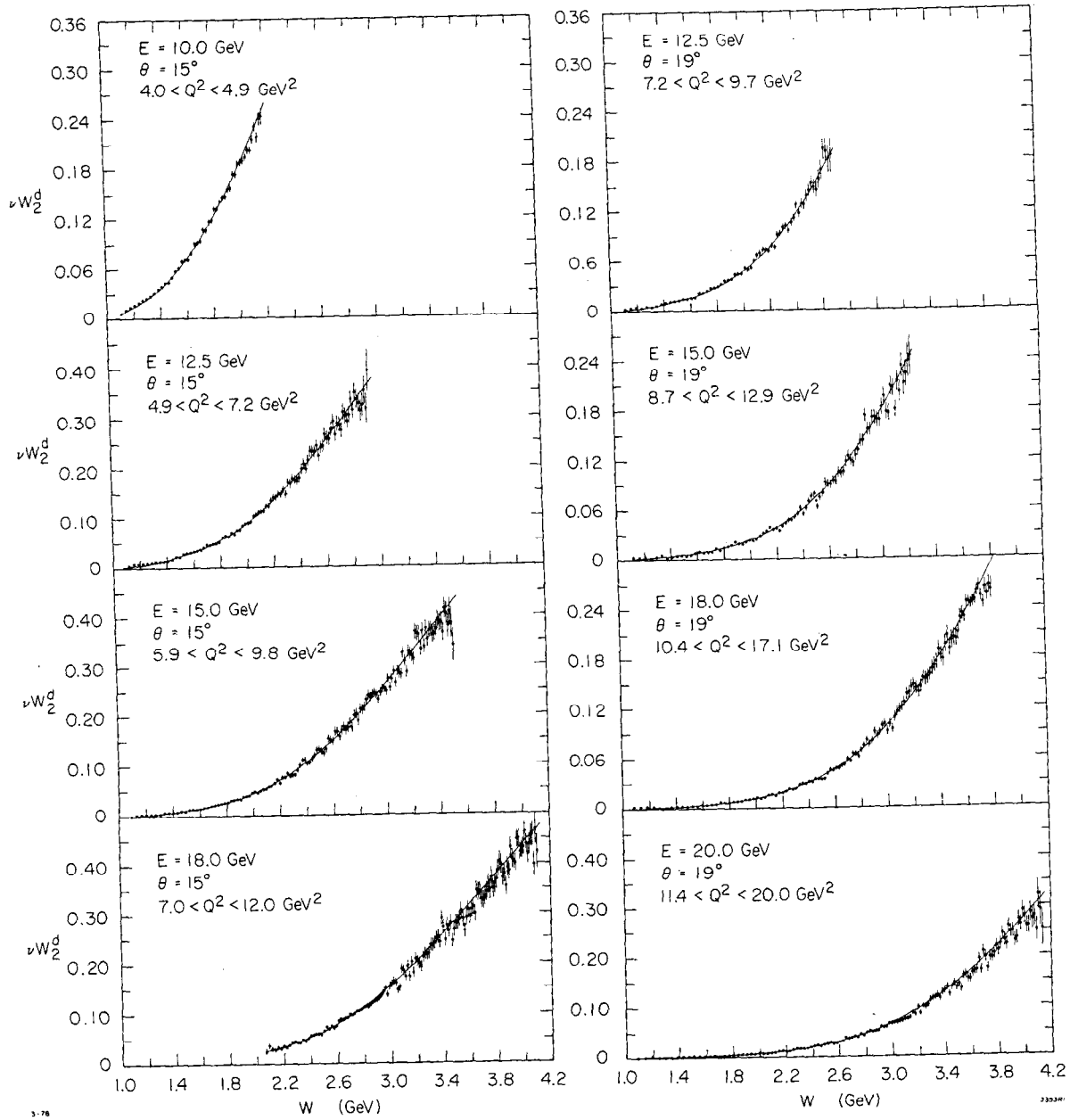


Fig. 15. The quantity νW_2^d extracted from inelastic $e - d$ cross sections measured at 15° and 19° in experiment B assuming $R_d = 0.18$.

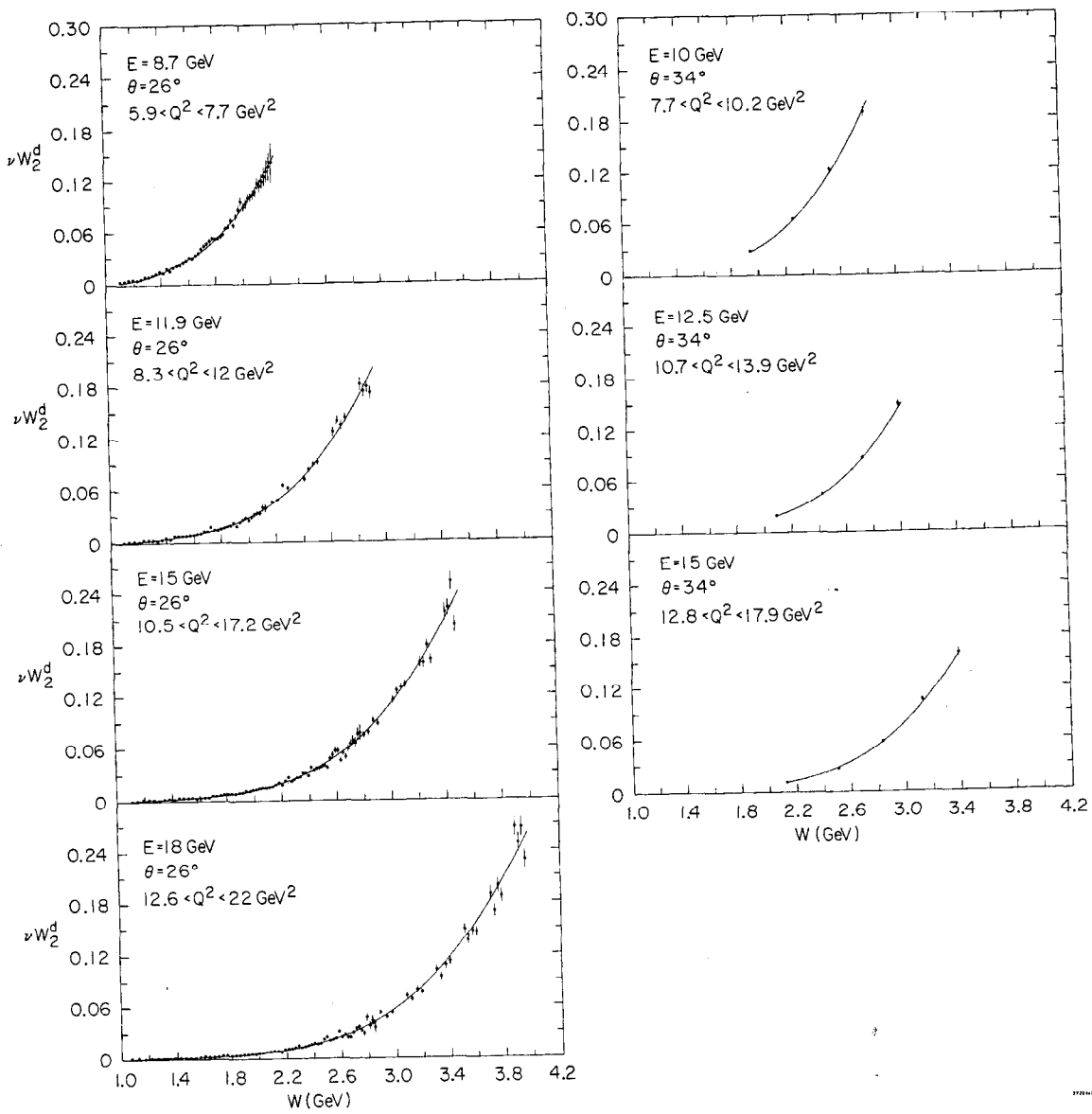


Fig. 16. The quantity νW_2^d extracted from inelastic $e - d$ cross sections measured at 26° and 34° in experiment B assuming $R_d = 0.18$.

by averaging several neighboring fine-mesh cross sections, as explained in section V.E. Treatment of the random and systematic errors is described in the following section.

The two experiments, A and B, were normalized to each other (see section V.F., following). In Table (V) we present the combined cross sections σ_p , σ_d , and σ_n as merged from experiments A and B. The cross sections from experiment B, where they existed for $\omega \lesssim 2$ at 26° and 34° , were used in lieu of those from experiment A. The errors given in Table (V) are one-standard-deviation random errors.

The statistical precision of our data in the resonance region is not as good as that of previous low Q^2 resonance cross section measurements (27, 28, 46, 59) at 4° , 6° , and 10° using the SLAC 20 GeV spectrometer. However, as these are the only high Q^2 resonance data currently available, we present some of them in Figures(17 through 20), which show the structure functions vW_2^p and vW_2^d again extracted from the cross sections assuming $R_p = R_d = 0.18$. Apparently, the cross section for resonance excitation is still relatively significant at the value of Q^2 measured here. The resonances in the vicinity of the $N^*(1520)$ and the $N^*(1688)$ resonances have excitation cross sections that appear to be the same fraction of the total cross section as at lower Q^2 . On the other hand, the cross section for the excitation of the $\Delta(1236)$ is dropping more rapidly with Q^2 than the non-resonant background cross section underneath it. The peak in the vicinity of the $N^*(1688)$ resonance appears to shift

TABLE V. Combined cross sections from experiments A and B.

E0 = 10.00 GEV

THETA = 14.991 DEG

NP	EP	W	SIGMA P	SIGMA D	SIGMA N
1	6.36	1.84	4727.8+-	95.2	7397.4+-
2	6.26	1.91	5465.1+-	96.7	8120.9+-
3	6.14	1.99	6237.3+-	106.7	9409.3+-
4	6.02	2.06	6953.9+-	109.2	10055.9+-
5	5.88	2.14	7657.9+-	134.0	11432.1+-

E0 = 12.50 GEV

THETA = 14.991 DEG

NP	EP	W	SIGMA P	SIGMA D	SIGMA N
1	7.64	1.87	1204.2+-	28.0	1752.4+-
2	7.46	2.00	1525.1+-	35.0	2282.1+-
3	7.27	2.13	2100.9+-	49.8	2959.5+-
4	7.06	2.26	2560.6+-	66.3	3678.2+-
5	6.84	2.38	2975.9+-	78.2	4390.8+-
6	6.62	2.51	3425.5+-	84.5	5326.9+-
7	6.38	2.63	3986.1+-	98.3	6149.2+-
8	6.14	2.75	4573.0+-	114.4	6823.3+-
9	5.90	2.87	4945.8+-	155.9	7554.6+-

E0 = 15.00 GEV

THETA = 14.991 DEG

NP	EP	W	SIGMA P	SIGMA D	SIGMA N
1	8.82	1.87	324.9+-	6.9	473.1+-
2	8.64	2.00	441.7+-	8.9	640.2+-
3	8.46	2.13	581.8+-	13.4	842.3+-
4	8.26	2.26	803.1+-	19.4	1076.6+-
5	8.04	2.40	983.2+-	25.1	1456.4+-
6	7.80	2.54	1278.6+-	30.2	1835.4+-
7	7.56	2.67	1476.6+-	27.9	2245.0+-
8	7.32	2.80	1669.8+-	33.4	2653.2+-
9	7.08	2.92	2010.6+-	45.9	3080.7+-
10	6.84	3.04	2220.4+-	49.4	3393.6+-
11	6.60	3.15	2399.0+-	52.6	3853.8+-
12	6.36	3.26	2694.1+-	57.4	4407.5+-
13	6.12	3.36	2848.8+-	60.8	4624.2+-
14	5.88	3.46	3134.8+-	86.4	4875.5+-

E0 = 18.00 GEV

THETA = 14.991 DEG

NP	EP	W	SIGMA P	SIGMA D	SIGMA N
1	9.68	2.16	183.0+-	9.0	248.9+-
2	9.48	2.29	225.3+-	7.1	338.5+-
3	9.30	2.41	294.6+-	7.7	425.8+-
4	9.12	2.52	373.4+-	8.6	531.1+-
5	8.94	2.63	462.2+-	7.8	662.3+-
6	8.78	2.73	534.3+-	8.1	762.9+-
7	8.61	2.82	594.3+-	8.8	855.5+-
8	8.43	2.92	682.9+-	12.9	951.2+-
9	8.24	3.02	766.1+-	19.8	1130.8+-
10	8.01	3.13	910.1+-	22.7	1380.3+-
11	7.77	3.25	1024.4+-	25.9	1540.6+-
12	7.53	3.36	1164.5+-	29.5	1831.6+-
13	7.29	3.47	1358.9+-	33.8	1964.7+-
14	7.05	3.58	1456.7+-	36.8	2137.9+-
15	6.81	3.68	1590.7+-	40.3	2398.1+-
16	6.57	3.78	1698.5+-	42.7	2660.1+-
17	6.33	3.88	1820.0+-	41.8	2841.6+-
18	6.09	3.97	1909.3+-	36.0	3150.9+-
19	5.85	4.06	2017.6+-	45.1	3243.9+-

The cross sections and their errors are in picobarns/steradian-GeV.

TABLE V continued.

E0 = 4.50 GEV THETA = 18.023 DEG

NP	EP	W	SIGMA P	SIGMA D	SIGMA N
1	2.60	1.81	68006.2+-	1180.9	120966.0+-
2	2.55	1.85	71785.4+-	1193.3	121351.0+-
3	2.51	1.88	72604.5+-	1145.3	124614.0+-
4	2.46	1.90	75018.4+-	1173.9	126486.0+-
5	2.41	1.93	72415.7+-	1185.4	124803.0+-
6	2.36	1.96	72584.2+-	1194.2	126035.0+-
7	2.31	1.99	73455.8+-	1292.8	126512.0+-
8	2.25	2.03	72428.1+-	1373.0	129445.0+-
9	2.00	2.17	71258.0+-	1586.8	127764.0+-
10	1.75	2.30	67920.3+-	1620.7	125274.0+-
11	1.50	2.42	67392.7+-	2332.0	122623.0+-
12	1.25	2.54	64626.3+-	2936.1	124708.0+-

E0 = 6.50 GEV THETA = 18.023 DEG

NP	EP	W	SIGMA P	SIGMA E	SIGMA N
1	3.88	1.82	14770.5+-	335.5	23450.4+-
2	3.81	1.87	15728.5+-	351.1	24853.4+-
3	3.61	2.00	19007.8+-	421.7	30058.6+-
4	3.50	2.07	19315.3+-	419.5	21662.8+-
5	3.38	2.14	20700.3+-	459.9	33798.5+-
6	3.26	2.21	21818.5+-	486.9	35895.7+-
7	3.10	2.30	21936.2+-	492.9	36857.3+-
8	2.99	2.36	22033.2+-	488.8	37895.5+-
9	2.85	2.43	23635.2+-	517.1	44096.6+-
10	2.70	2.51	24321.9+-	533.7	41515.8+-
11	2.50	2.61	23333.1+-	557.6	40244.8+-
12	2.36	2.67	23234.0+-	522.3	42581.7+-
13	2.28	2.71	23936.4+-	598.2	43414.7+-
14	2.19	2.75	21949.9+-	600.0	42514.4+-
15	2.11	2.79	23030.4+-	615.7	42341.8+-
16	2.00	2.84	25858.8+-	790.5	44367.0+-
17	1.50	3.05	26734.3+-	1296.5	51515.4+-

E0 = 8.60 GEV THETA = 18.023 DEG

NP	EP	W	SIGMA P	SIGMA D	SIGMA N
1	5.02	1.83	3200.4+-	61.4	
2	4.92	1.91	3823.1+-	79.8	
3	4.78	2.01	4511.4+-	88.8	
4	4.63	2.10	5225.9+-	88.4	
5	4.50	2.19	6090.3+-	113.2	
6	4.33	2.29	6563.5+-	129.9	
7	4.16	2.39	7271.3+-	142.3	
8	4.00	2.48	7755.9+-	180.2	
9	3.83	2.57	8463.9+-	181.1	
10	3.66	2.66	8909.8+-	189.0	
11	3.50	2.74	9331.6+-	190.2	
12	3.35	2.81	9988.9+-	206.9	
13	3.21	2.88	9803.0+-	209.7	
14	3.00	2.98	10604.6+-	221.1	
15	2.90	3.02	10877.0+-	247.3	
16	2.79	3.07	11178.4+-	263.0	
17	2.68	3.12	11033.5+-	256.0	
18	2.59	3.16	11403.5+-	270.7	
19	2.50	3.20	11378.1+-	282.9	
20	2.33	3.27	11275.2+-	335.2	
21	2.16	3.34	12086.9+-	358.8	
22	2.00	3.40	11899.0+-	433.7	
23	1.50	3.60	13693.7+-	1032.8	

TABLE V continued

$E_0 = 10.39$ GEV $\Theta = 18.023$ DEG

NP	EP	W	SIGMA P	SIGMA D	SIGMA N
1	5.75	1.93	1208.5+-	52.5	1827.7+-
2	5.49	2.11	1786.0+-	67.7	2633.9+-
3	5.25	2.28	2410.6+-	81.7	3535.3+-
4	4.99	2.43	2915.7+-	79.1	4356.5+-
5	4.75	2.58	3523.9+-	45.3	5452.7+-
6	4.50	2.71	4019.8+-	71.7	6484.8+-
7	4.31	2.81	4512.0+-	100.8	6896.0+-
8	4.12	2.91	4773.5+-	112.9	7386.3+-
9	3.93	3.00	5032.6+-	112.2	8208.7+-
10	3.79	3.07	5084.8+-	108.3	8589.0+-
11	3.64	3.14	5340.9+-	98.8	8970.3+-
12	3.50	3.20	5550.7+-	140.6	9487.9+-
13	3.35	3.27	5863.2+-	143.4	9846.5+-
14	3.19	3.34	6330.5+-	164.6	10294.4+-
15	3.00	3.42	6416.8+-	163.2	10963.1+-
16	2.84	3.49	6668.9+-	152.3	11344.8+-
17	2.69	3.55	6674.3+-	161.4	11707.9+-
18	2.50	3.63	6518.8+-	170.5	11657.9+-
19	2.32	3.70	7228.0+-	193.6	12657.6+-
20	2.13	3.77	6824.3+-	325.6	11804.2+-
21	2.00	3.82	7349.1+-	401.9	13430.4+-
22	1.79	3.90	8538.1+-	421.4	15295.3+-
23	1.50	4.01	9184.7+-	766.8	17537.8+-
					1161.8

$E_0 = 12.50$ GEV $\Theta = 18.023$ DEG

NP	EP	W	SIGMA P	SIGMA D	SIGMA N
1	5.91	2.45	1053.8+-	29.2	1539.7+-
2	4.94	3.00	2093.9+-	61.6	2369.0+-
3	4.12	3.40	2967.6+-	94.8	4775.2+-
4	3.31	3.75	3768.9+-	115.4	6222.2+-
5	2.94	3.90	3937.0+-	124.7	6864.0+-
6	2.69	4.00	4336.0+-	144.1	7502.9+-
7	2.43	4.10	4715.9+-	186.1	8128.6+-
8	2.25	4.17	4951.7+-	218.1	8801.2+-
9	2.07	4.23	5029.7+-	259.7	9214.2+-
10	1.88	4.30	5265.4+-	322.2	9759.9+-
11	1.74	4.35	5727.5+-	393.1	10366.7+-
12	1.60	4.40	5303.1+-	968.1	10725.1+-
					684.9

$E_0 = 13.30$ GEV $\Theta = 18.023$ DEG

NP	EP	W	SIGMA P	SIGMA D	SIGMA N
1	7.00	1.89	201.0+-	13.9	3C7.9+-
2	6.50	2.27	543.6+-	23.4	726.6+-
3	6.00	2.60	915.5+-	32.5	1439.0+-
4	5.75	2.75	1091.5+-	29.3	1729.1+-
5	5.50	2.89	1339.3+-	32.6	2052.7+-
6	5.25	3.02	1564.4+-	38.5	2502.9+-
7	5.00	3.15	1862.6+-	45.1	2862.5+-
8	4.75	3.28	1994.5+-	55.3	3298.0+-
9	4.50	3.40	2400.7+-	65.5	3607.6+-
10	4.27	3.50	2439.0+-	49.4	3900.7+-
11	4.00	3.62	2650.8+-	55.0	4329.7+-
12	3.82	3.70	2838.8+-	64.8	4599.4+-
13	3.68	3.76	2778.4+-	85.1	4758.9+-
14	3.50	3.83	2982.1+-	93.8	5227.3+-
15	3.34	3.90	3332.7+-	92.5	5411.1+-
16	3.09	4.00	3272.9+-	96.8	5700.0+-
					129.2

continued

1-79

3353841

TABLE V continued

E0 = 13.30 GEV THETA = 18.023 DEG (continued)

NP	EP	W	SIGMA P	SIGMA D	SIGMA N
17	2.92	4.07	3556.0+-	104.5	5836.0+-
18	2.74	4.14	3319.4+-	125.1	6429.8+-
19	2.63	4.18	3921.5+-	136.9	6617.8+-
20	2.50	4.23	3634.6+-	164.0	6979.9+-
21	2.31	4.30	4077.9+-	200.1	7532.9+-
22	2.00	4.41	4387.1+-	248.4	7846.9+-
23	1.93	4.44	4114.3+-	275.8	8057.3+-
24	1.78	4.49	4499.3+-	364.8	8376.1+-
25	1.67	4.53	4170.9+-	389.2	9679.3+-

E0 = 17.00 GEV THETA = 18.023 DEG

NP	EP	W	SIGMA P	SIGMA D	SIGMA N
1	7.99	2.11	62.3+-	1.7	93.6+-
2	7.50	2.49	146.6+-	3.7	213.7+-
3	7.00	2.83	272.2+-	7.7	404.2+-
4	6.50	3.12	430.6+-	10.1	672.3+-
5	6.00	3.40	627.4+-	17.5	942.1+-
6	5.75	3.52	741.2+-	21.6	1086.2+-
7	5.50	3.65	806.3+-	22.4	1308.2+-
8	5.35	3.72	881.7+-	25.5	1405.4+-
9	5.00	3.88	986.7+-	24.9	1594.5+-
10	4.75	3.99	1074.4+-	37.5	1815.0+-
11	4.50	4.10	1233.8+-	39.2	2051.1+-
12	4.25	4.21	1387.7+-	43.5	2315.6+-
13	4.00	4.31	1501.7+-	52.7	2511.1+-
14	3.75	4.42	1658.7+-	61.0	2746.5+-
15	3.50	4.51	1670.9+-	57.8	2841.6+-
16	3.33	4.58	1743.0+-	61.6	3112.4+-
17	3.15	4.65	1918.1+-	69.5	3229.5+-
18	3.00	4.71	2023.5+-	75.9	3436.4+-
19	2.75	4.80	1898.1+-	95.0	3605.9+-
20	2.50	4.89	2163.1+-	111.1	3797.1+-
21	2.22	4.99	2383.3+-	182.9	4359.4+-
22	2.00	5.07	2045.2+-	218.1	4997.7+-
23	1.82	5.13	2659.0+-	292.4	5017.8+-
24	1.77	5.15	2822.4+-	310.2	5118.7+-

E0 = 12.50 GEV THETA = 18.996 DEG

NP	EP	W	SIGMA P	SIGMA D	SIGMA N
1	6.43	1.87	216.5+-	5.4	319.8+-
2	6.25	2.02	322.3+-	7.2	442.7+-
3	6.07	2.16	443.3+-	9.8	633.7+-
4	5.88	2.30	598.3+-	12.6	820.4+-
5	5.65	2.45	765.2+-	16.8	1115.4+-
6	5.41	2.61	956.5+-	30.6	1443.8+-

E0 = 15.00 GEV THETA = 18.996 DEG

NP	EP	W	SIGMA P	SIGMA D	SIGMA N
1	7.27	1.87	52.3+-	2.0	86.1+-
2	7.09	2.03	89.2+-	2.5	123.3+-
3	6.91	2.18	131.5+-	3.9	185.7+-
4	6.73	2.33	178.9+-	5.5	252.1+-
5	6.55	2.46	225.5+-	7.0	331.7+-
6	6.36	2.59	313.3+-	8.4	433.2+-
7	6.13	2.74	388.0+-	9.4	560.0+-
8	5.89	2.89	502.5+-	12.2	756.3+-
9	5.65	3.03	619.8+-	15.4	902.2+-
10	5.41	3.17	741.9+-	22.3	1056.4+-

TABLE V continued

$E_C = 18.02 \text{ GEV}$

$\text{THETA} = 18.996 \text{ DEG}$

NP	EP	W	SIGMA P	SIGMA D	SIGMA N
1	8.15	1.85	12.9+-	0.5	22.7+-
2	8.00	2.00	20.8+-	0.6	33.0+-
3	7.79	2.19	36.1+-	0.9	51.7+-
4	7.55	2.39	55.9+-	1.5	83.4+-
5	7.31	2.58	84.6+-	2.2	119.6+-
6	7.07	2.75	119.1+-	3.0	174.8+-
7	6.83	2.91	162.5+-	4.1	246.1+-
8	6.59	3.07	207.7+-	5.2	305.5+-
9	6.35	3.21	250.3+-	6.5	406.0+-
10	6.11	3.35	340.6+-	8.5	481.4+-
11	5.87	3.49	380.4+-	9.1	571.7+-
12	5.63	3.62	446.2+-	6.4	697.8+-
13	5.39	3.74	511.0+-	7.6	774.5+-

$E_0 = 20.00 \text{ GEV}$

$\text{THETA} = 18.996 \text{ DEG}$

NP	EP	W	SIGMA P	SIGMA D	SIGMA N
1	8.60	1.88	6.3+-	0.2	12.0+-
2	8.40	2.08	12.6+-	0.4	19.0+-
3	8.19	2.28	20.7+-	0.6	31.2+-
4	7.98	2.46	31.1+-	0.9	46.8+-
5	7.76	2.64	47.6+-	1.3	68.2+-
6	7.52	2.82	69.1+-	1.8	97.6+-
7	7.28	2.98	93.6+-	2.4	133.0+-
8	7.04	3.14	124.2+-	3.2	168.7+-
9	6.80	3.29	166.9+-	4.3	228.6+-
10	6.56	3.44	197.6+-	5.2	283.9+-
11	6.32	3.58	238.1+-	6.2	336.4+-
12	6.08	3.71	274.4+-	7.4	413.9+-
13	5.84	3.84	333.6+-	9.0	501.3+-
14	5.60	3.96	377.1+-	10.4	570.6+-
15	5.36	4.09	404.7+-	15.9	626.0+-

$E_0 = 4.50 \text{ GEV}$

$\text{THETA} = 25.993 \text{ DEG}$

NP	EP	W	SIGMA P	SIGMA D	SIGMA N
1	2.00	1.94	13720.1+-	366.0	21740.0+-
2	1.80	2.08	15673.6+-	416.5	25083.4+-
3	1.60	2.21	16566.3+-	520.2	28064.9+-
4	1.40	2.33	17039.9+-	674.8	30607.4+-
5	1.20	2.45	19788.4+-	1234.2	32754.7+-

$E_0 = 6.70 \text{ GEV}$

$\text{THETA} = 25.993 \text{ DEG}$

NP	EP	W	SIGMA P	SIGMA D	SIGMA N
1	3.00	1.94	1868.1+-	57.1	2869.6+-
2	2.75	2.14	2699.7+-	84.1	4016.9+-
3	2.50	2.32	3466.5+-	106.9	5445.2+-
4	2.38	2.40	3733.7+-	116.2	5877.3+-
5	2.25	2.49	3870.0+-	128.9	6564.8+-
6	2.12	2.57	4383.9+-	152.8	7364.2+-
7	2.00	2.64	4985.8+-	152.6	7746.1+-
8	1.89	2.71	5218.1+-	165.3	8650.0+-
9	1.75	2.79	5519.9+-	199.6	9299.8+-
10	1.63	2.86	5640.8+-	225.1	9807.2+-
11	1.50	2.93	5624.2+-	308.6	10636.6+-
12	1.38	3.00	6902.6+-	391.8	11584.3+-

TABLE V continued

E0 = 8.70 GEV THETA = 25.993 DEG

NP	EP	W	SIGMA P	SIGMA D	SIGMA N
1	3.79	1.85	298.6+-	7.1	431.7+-
2	3.67	1.96	427.8+-	12.0	597.6+-
3	3.54	2.08	523.1+-	14.9	770.9+-
4	3.42	2.18	677.2+-	35.7	952.6+-
5	3.25	2.32	852.0+-	24.0	1289.6+-
6	3.00	2.51	1174.8+-	33.1	1831.9+-
7	2.75	2.68	1506.4+-	43.9	2433.1+-
8	2.50	2.85	1909.8+-	54.6	3071.3+-
9	2.39	2.92	2236.6+-	63.5	3412.6+-
10	2.27	2.99	2186.1+-	65.3	3372.1+-
11	2.14	3.07	2466.0+-	75.3	3846.5+-
12	2.00	3.15	2427.6+-	90.5	3795.6+-
13	1.88	3.22	2636.4+-	123.6	4821.7+-
14	1.75	3.29	2898.8+-	158.7	5161.7+-
15	1.50	3.43	3332.7+-	240.4	6241.1+-

E0 = 11.88 GEV THETA = 25.993 DEG

NP	EP	W	SIGMA P	SIGMA D	SIGMA N
1	4.61	1.86	36.7+-	1.7	54.5+-
2	4.52	1.96	48.9+-	1.9	68.6+-
3	4.41	2.07	70.3+-	3.2	97.4+-
4	4.25	2.23	107.1+-	3.2	160.8+-
5	4.00	2.46	170.8+-	4.6	246.9+-
6	3.75	2.67	258.0+-	7.0	405.0+-
7	3.50	2.86	370.3+-	10.3	535.4+-
8	3.25	3.04	502.6+-	15.0	770.0+-
9	3.00	3.21	615.0+-	18.9	1005.0+-
10	2.75	3.38	790.8+-	25.7	1244.2+-
11	2.50	3.53	908.4+-	30.9	1551.0+-
12	2.25	3.68	976.1+-	44.4	1718.0+-
13	2.13	3.75	1181.3+-	43.4	1931.2+-
14	2.00	3.82	1243.8+-	49.8	2192.9+-
15	1.67	4.00	1699.0+-	189.2	2736.7+-

E0 = 15.00 GEV THETA = 25.993 DEG

NP	EP	W	SIGMA P	SIGMA D	SIGMA N
1	5.18	1.89	8.1+-	0.3	13.2+-
2	5.04	2.07	14.3+-	0.4	20.7+-
3	4.89	2.24	21.1+-	0.6	31.8+-
4	4.73	2.41	32.8+-	0.9	47.9+-
5	4.57	2.56	48.2+-	1.5	68.4+-
6	4.41	2.71	64.8+-	2.3	94.2+-
7	4.25	2.86	89.8+-	2.4	127.3+-
8	4.00	3.06	129.9+-	3.1	196.0+-
9	3.75	3.26	182.6+-	4.6	264.1+-
10	3.50	3.44	240.3+-	7.2	371.2+-
11	3.25	3.61	296.2+-	11.7	482.7+-
12	3.00	3.78	377.5+-	14.5	607.6+-
13	2.75	3.94	454.7+-	18.5	746.1+-
14	2.50	4.09	528.1+-	19.7	851.6+-
15	2.39	4.16	590.3+-	27.0	942.9+-
16	2.25	4.24	607.4+-	33.0	1036.2+-
17	2.00	4.38	620.8+-	48.5	1259.2+-
18	1.75	4.52	905.6+-	62.6	1562.8+-

TABLE V continued

$E_0 = 18.02 \text{ GEV}$ $\text{THETA} = 25.993 \text{ DEG}$

NP	EP	W	SIGMA P	SIGMA D	SIGMA N
1	5.63	1.89	2.2+-	0.1	3.9+-
2	5.49	2.09	3.8+-	0.2	6.6+-
3	5.35	2.26	6.8+-	0.3	10.9+-
4	5.20	2.44	11.1+-	0.4	16.5+-
5	5.04	2.61	14.9+-	0.5	23.1+-
6	4.88	2.78	22.8+-	1.0	33.9+-
7	4.75	2.91	31.1+-	1.1	44.2+-
8	4.50	3.14	45.9+-	1.4	68.8+-
9	4.25	3.35	70.7+-	2.0	99.2+-
10	4.00	3.55	96.6+-	2.7	141.9+-
11	3.75	3.74	131.7+-	3.7	189.9+-
12	3.50	3.92	169.9+-	5.3	268.8+-
13	3.25	4.09	224.2+-	8.3	327.6+-
14	3.00	4.25	274.7+-	12.2	399.2+-
15	2.75	4.42	304.9+-	15.0	460.4+-
16	2.51	4.57	340.4+-	18.6	566.0+-
17	2.26	4.72	411.7+-	21.1	731.6+-
18	2.01	4.86	430.8+-	48.6	837.1+-
					67.4
					424.8+-
					83.7

$E_0 = 4.50 \text{ GEV}$ $\text{THETA} = 33.992 \text{ DEG}$

NP	EP	W	SIGMA P	SIGMA D	SIGMA N
1	1.60	1.97	4152.7+-	134.1	6161.4+-
2	1.40	2.13	4965.4+-	198.8	8225.9+-
3	1.20	2.29	6216.1+-	306.1	10296.5+-
					395.1
					4327.3+-
					486.5

$E_0 = 5.80 \text{ GEV}$ $\text{THETA} = 33.992 \text{ DEG}$

NP	EP	W	SIGMA P	SIGMA D	SIGMA N
1	2.00	2.01	1149.4+-	37.8	1771.2+-
2	1.75	2.24	1805.0+-	58.7	2872.1+-
3	1.50	2.44	2542.8+-	92.1	3965.4+-
4	1.25	2.63	3280.7+-	170.2	5336.0+-
					229.5
					2177.4+-
					280.2

$E_0 = 7.90 \text{ GEV}$ $\text{THETA} = 33.992 \text{ DEG}$

NP	EP	W	SIGMA P	SIGMA D	SIGMA N
1	2.50	2.07	217.0+-	9.2	343.8+-
2	2.25	2.33	411.3+-	14.3	590.4+-
3	2.00	2.56	642.5+-	23.4	927.3+-
4	1.75	2.77	924.6+-	32.1	1422.0+-
5	1.48	2.99	1301.6+-	54.1	2180.1+-
					82.1
					932.9+-
					95.4

$E_0 = 10.00 \text{ GEV}$ $\text{THETA} = 33.992 \text{ DEG}$

NP	EP	W	SIGMA P	SIGMA D	SIGMA N
1	3.00	1.94	35.1+-	1.2	51.5+-
2	2.75	2.26	80.3+-	2.5	120.8+-
3	2.50	2.53	173.9+-	5.5	236.3+-
4	2.25	2.78	257.4+-	10.6	384.3+-
5	2.00	3.01	409.4+-	19.9	583.2+-
6	1.75	3.22	566.2+-	27.4	857.7+-
7	1.50	3.42	820.3+-	40.7	1260.5+-
					47.2
					471.2+-
					60.6

TABLE V continued

EC = 12.50 GEV THETA = 33.992 DEG

NP	EP	W	SIGMA P	SIGMA D	SIGMA N			
1	3.25	2.09	12.8+-	0.5	18.6+-	0.6	3.8+-	0.6
2	3.00	2.43	31.3+-	1.0	44.8+-	1.2	12.4+-	1.5
3	2.75	2.73	64.7+-	2.0	89.9+-	2.4	26.0+-	3.1
4	2.50	2.99	107.9+-	3.7	164.0+-	4.4	59.7+-	6.0
5	2.25	3.24	180.5+-	9.1	255.3+-	8.3	81.8+-	11.9
6	2.00	3.47	218.8+-	11.3	382.2+-	12.6	174.0+-	16.4
7	1.75	3.68	372.2+-	20.5	512.1+-	21.4	153.5+-	29.1

EC = 15.00 GEV THETA = 33.992 DEG

NP	EP	W	SIGMA P	SIGMA D	SIGMA N			
1	3.50	2.13	4.1+-	0.2	6.4+-	0.3	1.2+-	0.3
2	3.25	2.50	11.5+-	0.4	16.0+-	0.5	3.6+-	0.6
3	3.00	2.83	25.0+-	0.9	36.7+-	1.0	11.3+-	1.3
4	2.75	3.13	47.1+-	1.6	70.7+-	1.9	24.4+-	2.6
5	2.50	3.39	79.8+-	2.8	114.9+-	3.5	37.7+-	4.6
6	2.25	3.64	105.6+-	8.7	179.8+-	8.6	79.1+-	12.1
7	2.00	3.88	144.6+-	12.8	239.9+-	16.1	102.0+-	20.6

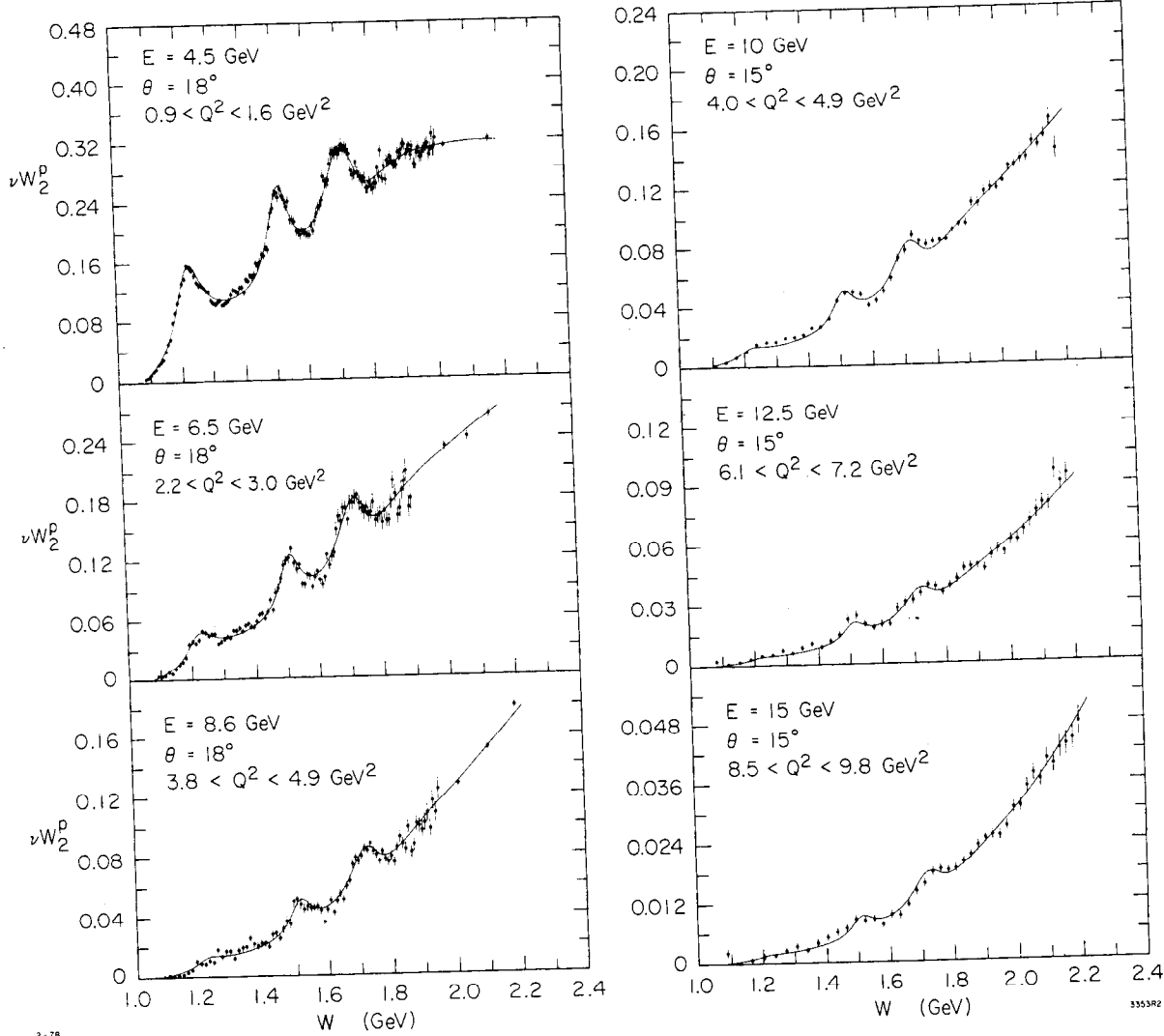


Fig. 17. The quantity νW_2^p measured at 18° and 15° in the resonance region.

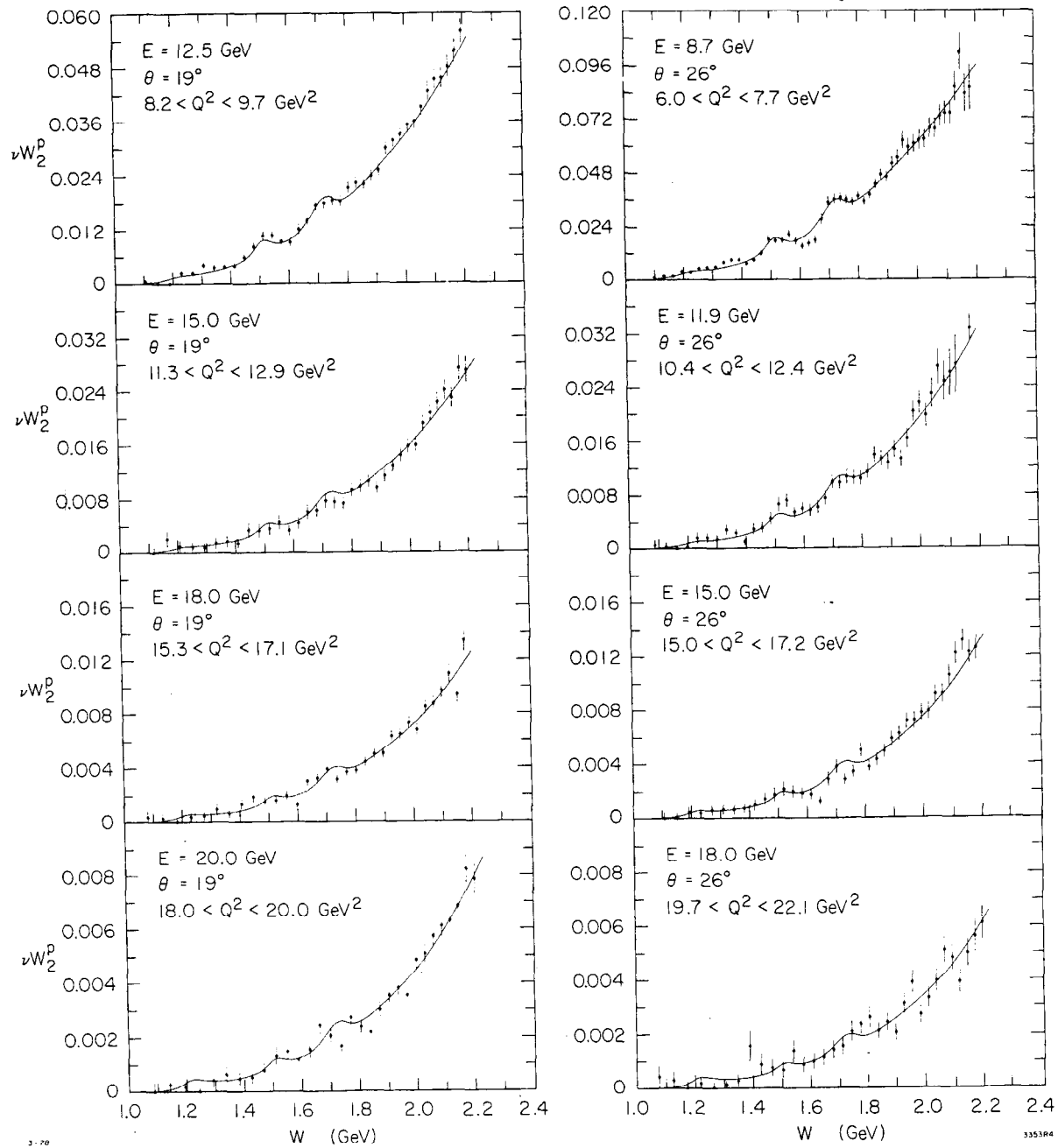


Fig. 18. The quantity vW_2^p measured at 19° and 26° in the resonance region.

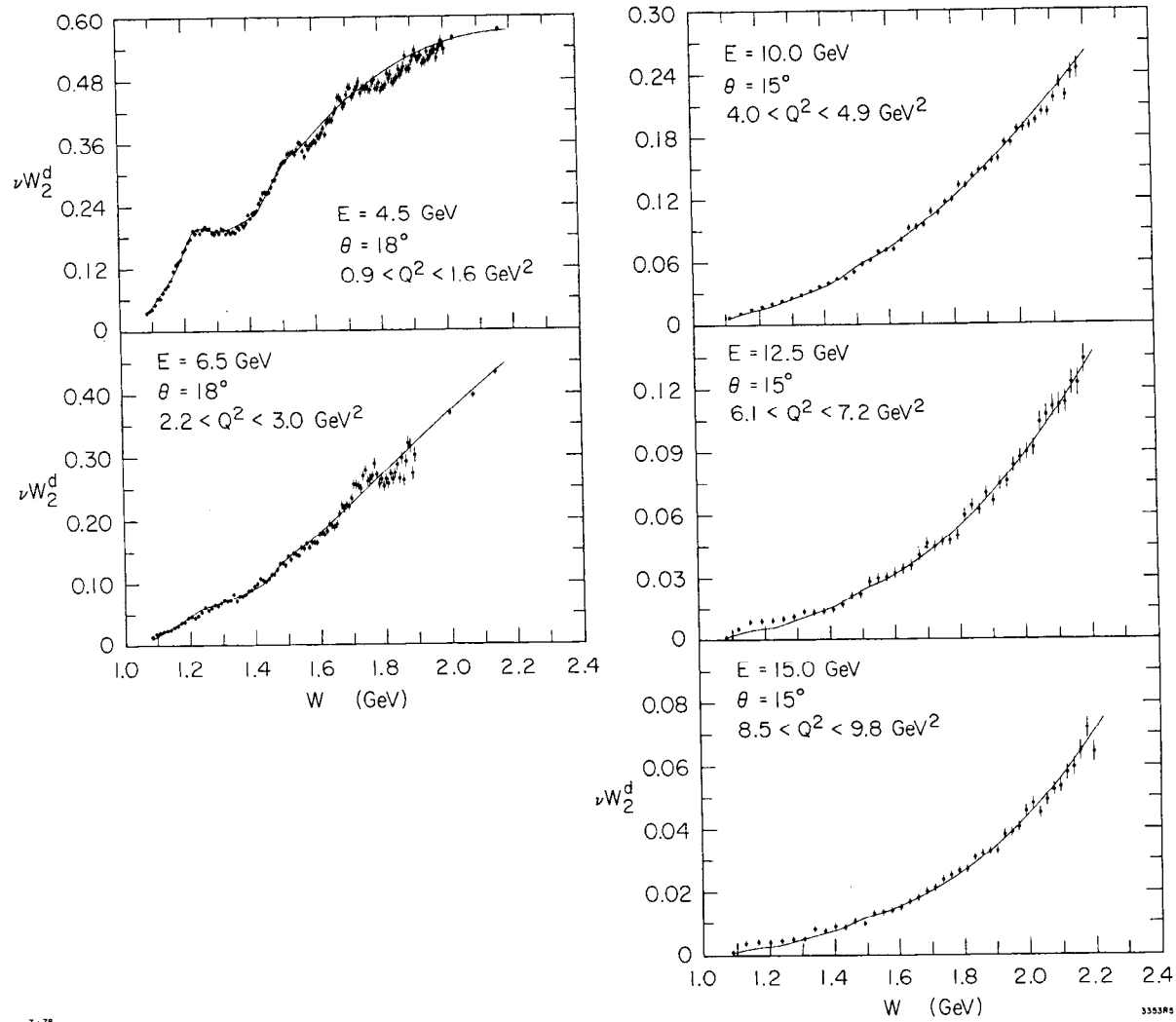


Fig. 19. The quantity νW_2^d measured at 18° and 15° in the resonance region.

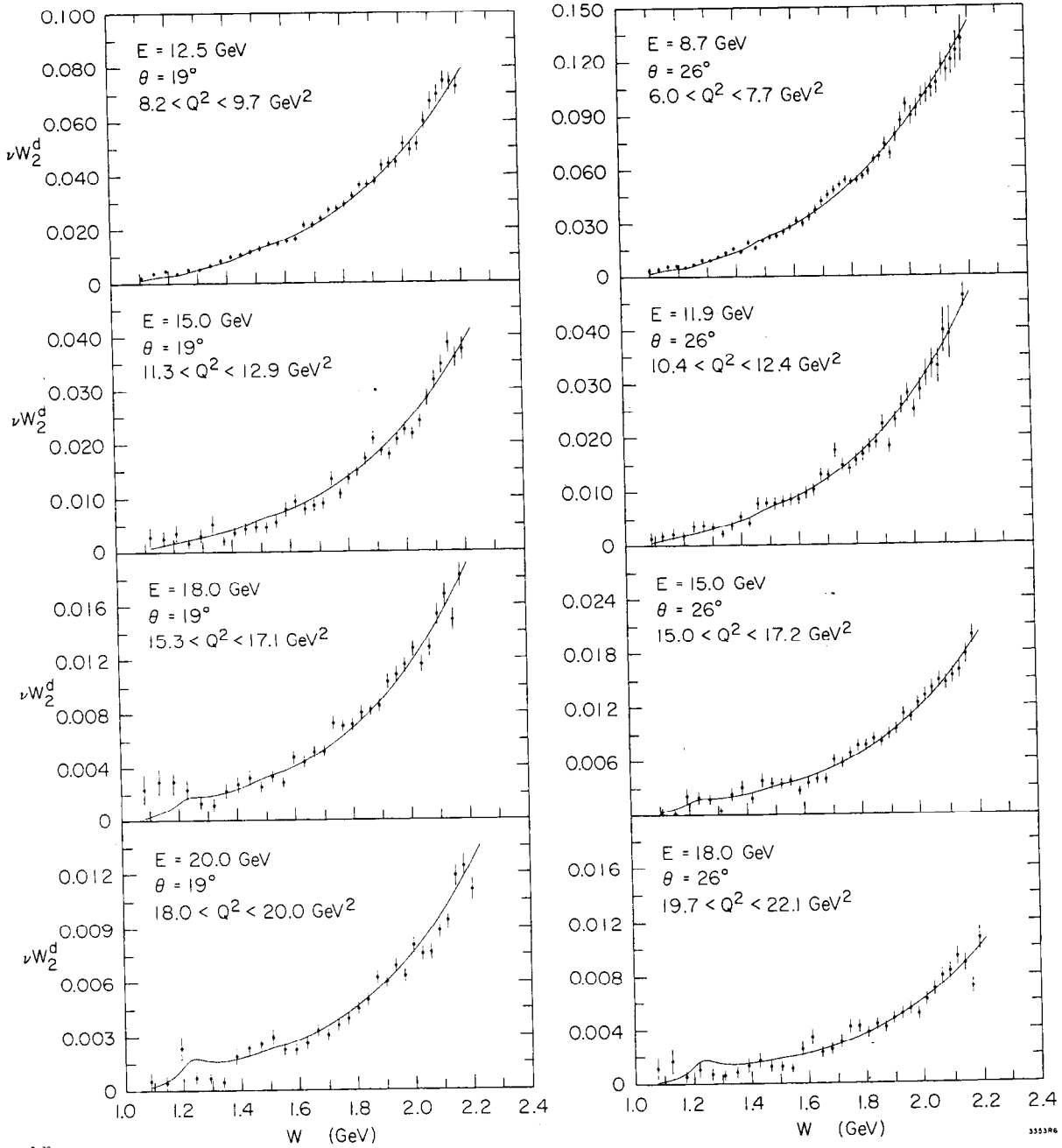


Fig. 20. The quantity νW_2^d measured at 19° and 26° in the resonance region.

to higher W with increasing Q^2 , indicating that several partial wave amplitudes are probably contributing to this peak. As is the case at low Q^2 , no prominent excitation of the $\Delta(1920)$ is seen in these spectra.

V.B. Error Summary

The random errors quoted in Table V arise from counting statistics and the possible random fluctuations in the properties of the beam, target apparatus, spectrometer, and the various monitors. These contributions are summarized in Table VI ; percentage errors in the final cross sections arising from these sources are given.

The random error arising from counting statistics normally dominates the error from random fluctuations, which is typically 1% when all the contributions B.a - B.g are added in quadrature. These fluctuation errors were not reduced in the process of combining several experimental runs if the measurements were made over a time span which was short in comparison to the time scale of the fluctuations. Nor were these errors reduced when data from different missing energy bins of the same run were combined into a single cross section for inclusion in Table (V). Only the errors arising from counting statistics were reduced in combining the fine-mesh cross sections (see section V.E.). As the measurements with hydrogen and deuterium targets had been interleaved in time, only errors from counting statistics and target density fluctuations were included when calculating the random errors in the ratio σ_d/σ_p .

Table VI. Random errors in cross sections

Source of error	Percentage error in σ
A. Counting Statistics	
a. Statistical errors in full target e-p and e-d cross sections	1.0 - 15.0
b. Statistical errors in empty replica target cross sections	0.1 - 1.5
c. Statistical errors in positron cross sections	0.0 - 0.3
d. Statistical errors in detector efficiencies	0.5 - 1.5
B. Random Fluctuations in Apparatus	
a. Target density fluctuations	0.3
b. Charge monitor fluctuations	0.3
c. Fluctuations in incident beam energy	0.1 - 0.8
d. Fluctuations in incident beam direction	0.1 - 1.1
e. Errors in setting spectrometer angle	0.1 - 0.5
f. Fluctuations in spectrometer magnet currents	0.0 - 0.5
g. Fluctuations in detector efficiencies	0.5 - 1.0

Systematic uncertainties in the e-p and e-d cross sections also fall into two categories: those that affect only the overall normalization of either experiment, or those which could also have a kinematic variation. These are listed in Table (VII) with typical estimates of each uncertainty.

Added in quadrature, the above systematic uncertainties yield an overall normalization uncertainty of 3.4 - 3.6% in the proton and deuteron cross sections. In addition, there is a point-to-point relative uncertainty of not more than 5.5% in these cross sections. When data from experiments A and B were merged for presentation in Table (V) and then used in conjunction with the 6° and 10° data^(27,28) of experiment C to extract R, the cross sections were modified by normalization factors (see section V.F) that attempted to account for normalization differences among the three experiments arising from sources A.a - A.f in Table (VII). Therefore, the systematic uncertainty in R must arise from the uncertainties in these normalization factors and from the sources B.a - B.f in Table (VII). Most of the systematic uncertainties, however, cancel in the ratio σ_d/σ_p from which σ_n/σ_p is derived (see section V.D). Those that do not are the uncertainties in target lengths and densities.

V.C. Global Fit

We have obtained universal fits to the structure functions vW_2^P and vW_2^d , using the data shown in Figures (9 - 16) together

Table VII. Systematic uncertainties in cross sections

Source of uncertainty	Percentage uncertainty in σ
A. Overall Normalization Uncertainties	
a. Calibration of spectrometer acceptance	1.5
b. Calibration of charge monitors	0.5
c. Target density normalization (hydrogen)	0.4 ^b - 0.7 ^a
d. Target density normalization (deuterium)	0.7 ^b - 0.9 ^a
e. Target length determination	0.4 ^b - 0.6 ^a
f. Target impurities	0.1
g. Radiative correction uncertainty	3.0
B. Relative Uncertainties	
a. Calibration of incident energy	0.1 - 0.8
b. Calibration of E' versus E	0.1 - 1.0
c. Acceptance averaging correction	0.0 - 1.0
d. Variation with E' of spectrometer acceptance	0.0 - 1.0
e. Electron detection efficiency	0.5 - 1.0
f. Radiative correction uncertainty	1.0 - 5.0

^aExperiment A only

^bExperiment B only

with similar data⁽²⁷⁾ from experiment C. As $R_p = R_d = 0.18$ was assumed to extract vW_2 from cross sections for the purpose of the fits, these fits are best used to provide an adequate representation of the inelastic e-p and e-d cross sections in the kinematic regions measured in these three experiments. The fitting program, as well as the explicit functional form of the fits were due to Atwood and Stein.^(59, 60) The quantity vW_2 was parameterized as follows⁽⁶¹⁾

$$vW_2(v, Q^2) = A(W, Q^2) f(\omega_w)/\omega$$

where

$$f(\omega_w) = \omega_w \sum_{n=3}^7 C_n (1 - \frac{1}{\omega_w})^n \quad (v.1)$$

and

$$\omega_w = \frac{2Mv + a^2}{Q^2 + b^2}$$

The modulating function $A(W, Q^2)$ contained 12 parameters representing the masses, widths, and amplitudes of the cross sections for electroproduction of the four most prominent nucleon resonances, and 8 parameters representing the W dependence of the non-resonant background under these resonances.

This modulating function was close to unity for $W > 2.0$. Indeed, for $W > 2.5$ GeV, $|A(W, Q^2) - 1| \leq 0.01$. vW_2 was essentially equal to $f(\omega_w)/\omega$. The scaling variable ω_w , first proposed by Rittenberg and Rubinstein⁽⁶²⁾, extends scaling of vW_2 down to values of Q^2 near 0.1 GeV². The parameters $C_1 = a^2$, $C_2 = b^2$, C_3 through C_7 , and most of the 24 parameters in

$A(W, Q^2)$ were determined simultaneously by performing least square fits of the form given in equation (V.1) to all the data for vW_2^P and vW_2^D from the three experiments. Data from the line of lowest E at each scattering angle in experiments A and C were not included in this sample, however, because of uncertainties in the radiative corrections having to do with extrapolations of the uncorrected cross sections to low E (see section IV.D.5). In the case of the deuteron, the function $f(\omega_w)$ had an additional multiplicative factor $[1 - e^{-7.7(\omega' - 1)}]^{-1}$ included to account for deuteron binding effects at small $\omega' = \omega + M^2/Q^2$. Best fit values of C_1 through C_7 are given in Table (VIII) for the proton and deuteron. Also given in this table are values of these parameters for fits to the neutron data discussed in section V.D.

These functional forms provided reasonable fits to the proton and deuteron cross sections, especially in the deep inelastic region. Values of χ^2 per degree of freedom were 1.59 (2533 data points) for the proton and 1.96 (2303 data points) for the deuteron. Most of the difficulty in fitting the data occurred in the resonance region; the χ^2 per degree of freedom was 1.2 for the proton and 1.4 for the deuteron when the fits were restricted to $W \geq 1.8$ GeV. The accuracy of these fits in modeling the data is seen graphically in

Table VIII. Global fit parameters

	Proton	Deuteron	Neutron
$c_1 = a^2$	1.642 ± 0.011	1.512 ± 0.009	1.642 ± 0.011^a
$c_2 = b^2$	0.376 ± 0.005	0.351 ± 0.004	0.376 ± 0.005^a
c_3	0.256	0.477	0.064
c_4	2.178	2.160	0.225
c_5	0.898	3.627	4.106
c_6	-6.716	-10.470	-7.079
c_7	3.756	4.927	3.055

^aheld equal to value from proton fit

figures (9 - 20). Their relevance in regions not yet measured in the SLAC experiments is subject to the assumptions implicit in the fit (mostly the scaling assumption). We emphasize that $R_p = R_d = 0.18$ was assumed to extract vW_2 for these fits, and advise that this assumption should be used with these fits to reconstruct the cross section in the deep inelastic region.

V.D. Neutron Cross Sections

V.D.1. Introduction

Cross sections for inelastic e-n scattering were extracted from the e-d cross sections using an impulse approximation. The method used is that of Atwood and West^(19), with small modifications for off-mass-shell effects.^(20, 63) In this method, the electron is assumed to scatter incoherently from the proton and neutron, and corrections for Fermi motion of the nucleons within the deuteron, commonly known as smearing corrections, are made. Corrections to the impulse approximation are believed to be small^(19, 20) at the large values of Q^2 of these experiments. In this section we outline the procedure used in the extraction of e-n cross sections from the e-d data. A detailed discussion of deuteron binding effects is reserved for Appendix III .

V.D.2. Smeared Proton Cross Sections

The first step in the extraction of the neutron cross sec-

tions was the introduction of Fermi-motion effects into the measured proton cross sections. The assumption $R_p = 0.18$ was used together with the global fit to νW_2^P to provide parameterizations of the two proton structure functions needed in this step. The proton structure functions from this fit were integrated over the momentum distribution of the proton within the deuteron to produce the "smeared" proton structure functions^(19, 20) W_{1s}^P and W_{2s}^P

$$W_{1s}(\nu, Q^2) = \int d^3\vec{p} |f(\vec{p})|^2 \left\{ W_1^P(\nu', Q^2, W') + W_2^P(\nu', Q^2, W') \frac{\vec{p}^2 - P_3^2}{2M^2} \right\}$$

$$W_{2s}(\nu, Q^2) = \int d^3\vec{p} |f(\vec{p})|^2 \left\{ \frac{1 - P_3 Q^2}{M\nu' q_3} \left(\frac{\nu'^2}{\nu} + \left(\frac{\vec{p}^2 - P_3^2}{2M} \right) \frac{Q^2}{q_3^2} \right) W_2^P(\nu', Q^2, W') \right\} \quad (V.2)$$

As detailed in Appendix III, p is the four-momentum of the proton (off the mass shell), $q = (0, 0, q_3, \nu)$ is the four momentum of the virtual photon, $\nu' = p \cdot q / M$, $(W')^2 = (p+q)^2$, and $|f(\vec{p})|$ is the momentum distribution of a nucleon within the deuteron, taken to be the square of the Fourier transform of the non-relativistic wave function. Aside from small off-mass-shell corrections (see Appendix III) the structure functions W_1^P and W_2^P used in equation V.2 are identified with the measured on-shell structure functions at the same values of Q^2 and $W=W'$.

The smeared structure functions were combined as in equation (I.1) to yield a smeared fit proton cross section σ_{ps}^f at each experimental point. The ratio of the fit cross section

before smearing σ_p^f to the smeared fit cross section,

$S_p = \sigma_p^f / \sigma_{ps}^f$, was taken to be the proton smearing correction.

The experimental proton cross sections $\sigma_p = (\frac{d^2\sigma}{dQdE})_p$ were then divided by S_p to yield the smeared proton cross sections

$$\sigma_{ps} = \sigma_p / S_p.$$

The quantity S_p and the corresponding ratios for the individual structure functions $S_{p1} = w_1^p / w_{1s}^p$ and $S_{p2} = w_2^p / w_{2s}^p$ are nearly identical (see Appendix III) and insensitive to the value of R assumed as long as the parameterizations used provide good representations of the two structure functions. The quantity S_p varies sharply with x for $x \geq 0.6$, while for fixed values of x , S_p varies only weakly with Q^2 . As an example of the x -dependences in the 20 GeV, 19° measurements of experiment B, S_p was 1.028, 1.026, 1.010, 0.982, 0.880, and 0.710 for x of 0.413, 0.538, 0.640, 0.710, 0.810, and 0.883 respectively.

V.D.3. Unsmeared Neutron Cross Sections

Subtraction of the smeared proton cross section from the deuteron cross section measured at the same kinematics yielded the smeared neutron cross section $\sigma_{ns} = \sigma_d - \sigma_{ps}$. The smeared cross section ratio σ_{ns}/σ_{ps} was then

$$\frac{\sigma_{ns}}{\sigma_{ps}} = S_p \frac{\sigma_d}{\sigma_p} - 1 \quad (V.3)$$

This smeared ratio is equal to the true ratio σ_n/σ_p only if

the neutron smearing correction $S_n = \sigma_n/\sigma_{ns}$ is equal to S_p .

We removed the smearing effects from the smeared neutron cross section and from the smeared ratio by calculating S_n and forming the unsmeareding correction factor $U = S_n/S_p$. The unsmeared neutron cross sections were then calculated from

$$\sigma_n = \sigma_{ns} S_n = S_n \sigma_p - U \sigma_p \quad (V.4)$$

and the unsmeared cross section ratio was

$$\frac{\sigma_n}{\sigma_p} = U \left(\frac{\sigma_{ns}}{\sigma_{ps}} \right) = U \left(S_p \frac{\sigma_p}{\sigma_p} - 1 \right) \quad (V.5)$$

Values of the unsmeareding correction U and the neutron smearing correction S_n were calculated by an unfolding procedure that employed a best fit method. The structure function W_2^n was assumed to have the same general functional form as given for the proton in equation (V.1). The 24 parameters in $A(W, Q^2)$ and the parameters $C_1 = a^2$ and $C_2 = b^2$ in ω_w were assumed to be equal to the corresponding parameters for the proton. As $A(W, Q^2)$ was essentially unity in the deep inelastic region, this assumption had little effect on our results. Under these assumptions, the structure function W_2^n was represented by a polynomial in $(1-\omega_w)$ with five undetermined coefficients. The individual terms in the polynomial were then smeared according to equation (V.2) and the coefficients C_3 through C_7 determined by fitting σ_{ns}^f calculated with this smeared structure function to the measured values of σ_{ns} . The assumption

$R_n = R_{ns} = 0.18$ was also used in these calculations to get σ_n^f and σ_{ns}^f from fits to the structure functions W_2^n and W_{2s}^n , but the results were insensitive to the particular form of R_n used. The constraints $\sigma_n^f/\sigma_p^f = 1.0$ at $1/\omega_w = 0$ and $\sigma_n^f/\sigma_p^f = 0.25$ at $\omega_w = 1$ were also imposed during the fitting procedure to ensure a representation of σ_n^f that could be extrapolated reliably. These constraints, however, had insignificant effects on the results. The extracted values of the cross section ratios σ_n/σ_p and the associated uncertainties due to the various assumptions in the unsmeared fit are given in Tables (IX) and (X). The correction factors $S_n = \sigma_n^f/\sigma_{ns}^f$ and $U = S_n/S_p$ were finally evaluated at the kinematic values of the e-p and e-d measurements using the values of the fit cross sections there. The unsmeared correction, U , was not far from unity, varying from 0.90 ± 0.02 at the smallest value of ω measured in the deep inelastic region to 1.002 ± 0.003 at the largest measured value of ω .

This unsmeared procedure was reliable only in the deep inelastic region where the structure functions vary smoothly with no resonant structure. The above method was not used in the resonance region because the structure functions are non-linear in the undetermined resonance parameters and we could not solve for these parameters by smearing a linear set of functions. Only when the parameterization of the structure functions is

Table IX. Ratios σ_n/σ_p from experiment A

x, x'	$\sigma_n/\sigma_p(x)$	$\sigma_n/\sigma_p(x')$
0.085	0.973 \pm 0.183	0.968 \pm 0.183
0.115	0.892 \pm 0.050	0.886 \pm 0.049
0.145	0.786 \pm 0.035	0.839 \pm 0.030
0.175	0.853 \pm 0.027	0.804 \pm 0.025
0.205	0.774 \pm 0.025	0.754 \pm 0.025
0.235	0.726 \pm 0.025	0.733 \pm 0.025
0.265	0.751 \pm 0.026	0.704 \pm 0.022
0.295	0.687 \pm 0.022	0.678 \pm 0.022
0.325	0.671 \pm 0.023	0.642 \pm 0.022
0.355	0.646 \pm 0.023	0.638 \pm 0.023
0.385	0.633 \pm 0.023	0.623 \pm 0.025
0.415	0.632 \pm 0.023	0.635 \pm 0.024
0.445	0.620 \pm 0.023	0.561 \pm 0.026
0.475	0.570 \pm 0.028	0.547 \pm 0.028
0.505	0.550 \pm 0.028	0.552 \pm 0.026
0.535	0.563 \pm 0.028	0.534 \pm 0.027
0.565	0.535 \pm 0.028	0.498 \pm 0.036
0.595	0.494 \pm 0.033	0.494 \pm 0.035
0.625	0.499 \pm 0.032	0.451 \pm 0.033
0.655	0.455 \pm 0.033	0.433 \pm 0.036
0.685	0.423 \pm 0.052	0.403 \pm 0.055
0.715	0.417 \pm 0.036	0.319 \pm 0.066
0.745	0.318 \pm 0.066	
0.775		0.367 \pm 0.040 ^a
0.805	0.370 \pm 0.040 ^a	

^aData for two intervals combined.

Table X. Ratios σ_n/σ_p from experiment B

Systematic uncertainties

x, x'	Target	"Wave function"	"Off shell"	"Fit"	$\sigma_n/\sigma_p(x)$	$\sigma_n/\sigma_p(x')$
0.305		0.017	0.001	0.001	0.647 \pm 0.058	0.631 \pm 0.038
0.335		0.017	0.002	0.001	0.663 \pm 0.033	0.656 \pm 0.031
0.365		0.016	0.002	0.001	0.620 \pm 0.031	0.618 \pm 0.031
0.395		0.016	0.002	0.002	0.643 \pm 0.032	0.596 \pm 0.028
0.425		0.016	0.003	0.002	0.555 \pm 0.026	0.547 \pm 0.023
0.455		0.016	0.004	0.002	0.565 \pm 0.022	0.585 \pm 0.021
0.485		0.016	0.004	0.003	0.594 \pm 0.023	0.541 \pm 0.020
0.515		0.016	0.005	0.004	0.536 \pm 0.022	0.513 \pm 0.020
0.545		0.015	0.005	0.004	0.503 \pm 0.020	0.514 \pm 0.020
0.575		0.015	0.006	0.004	0.523 \pm 0.020	0.464 \pm 0.019
0.605		0.015	0.006	0.005	0.472 \pm 0.019	0.454 \pm 0.019
0.635		0.015	0.007	0.006	0.460 \pm 0.019	0.450 \pm 0.020
0.665		0.015	0.008	0.007	0.454 \pm 0.021	0.398 \pm 0.019
0.695		0.014	0.010	0.008	0.431 \pm 0.020	0.398 \pm 0.021
0.725		0.014	0.012	0.009	0.376 \pm 0.020	0.362 \pm 0.020
0.755		0.013	0.014	0.010	0.391 \pm 0.021	0.335 \pm 0.023
0.785		0.013	0.015	0.011	0.337 \pm 0.020	0.310 \pm 0.024
0.815		0.012	0.016	0.012	0.304 \pm 0.024	0.270 \pm 0.026
0.845		0.012	0.018	0.014	0.281 \pm 0.025	0.291 \pm 0.041 ^a
0.875		0.012	0.020	0.017	0.313 \pm 0.034	

^aData for 2 intervals combined.

linear in the undetermined coefficients can they be taken out of the smearing integrals, and the smearing process decoupled from the fitting procedure. We therefore quote neutron cross sections only for $W \geq 1.8$ GeV. The neutron cross sections are represented in Figures (21 - 24) by the neutron structure function vW_2^N extracted from σ_n under the assumption $R_n = 0.18$. The neutron cross sections themselves are presented in Table (V), along with the proton and deuteron cross sections. As is the case for e-p and e-d cross sections, only combined cross sections are given in the tables. The combination of fine-mesh neutron cross sections used a procedure similar to that used for the proton and deuteron, as discussed in the next section. The cross section ratios σ_n/σ_p were calculated directly from the fine-mesh deuteron and proton cross sections according to equation (V.5), and later combined according to the procedure described below.

The values of σ_n/σ_p as functions of x , and separately x' , given in Tables (IX) and (X), are shown in Figure (25). The ratios were calculated at all measured kinematic points with $W \geq 1.8$ GeV and $Q^2 \geq 1.0$ GeV 2 (see Figures 9 - 12 and 21-24) and averaged in small intervals of x or $x' = 1/\omega'$ ($\Delta x = 0.03$). In this averaging it is assumed that σ_n/σ_p approximately scales in x or x' (see section VII). The data of the two experiments

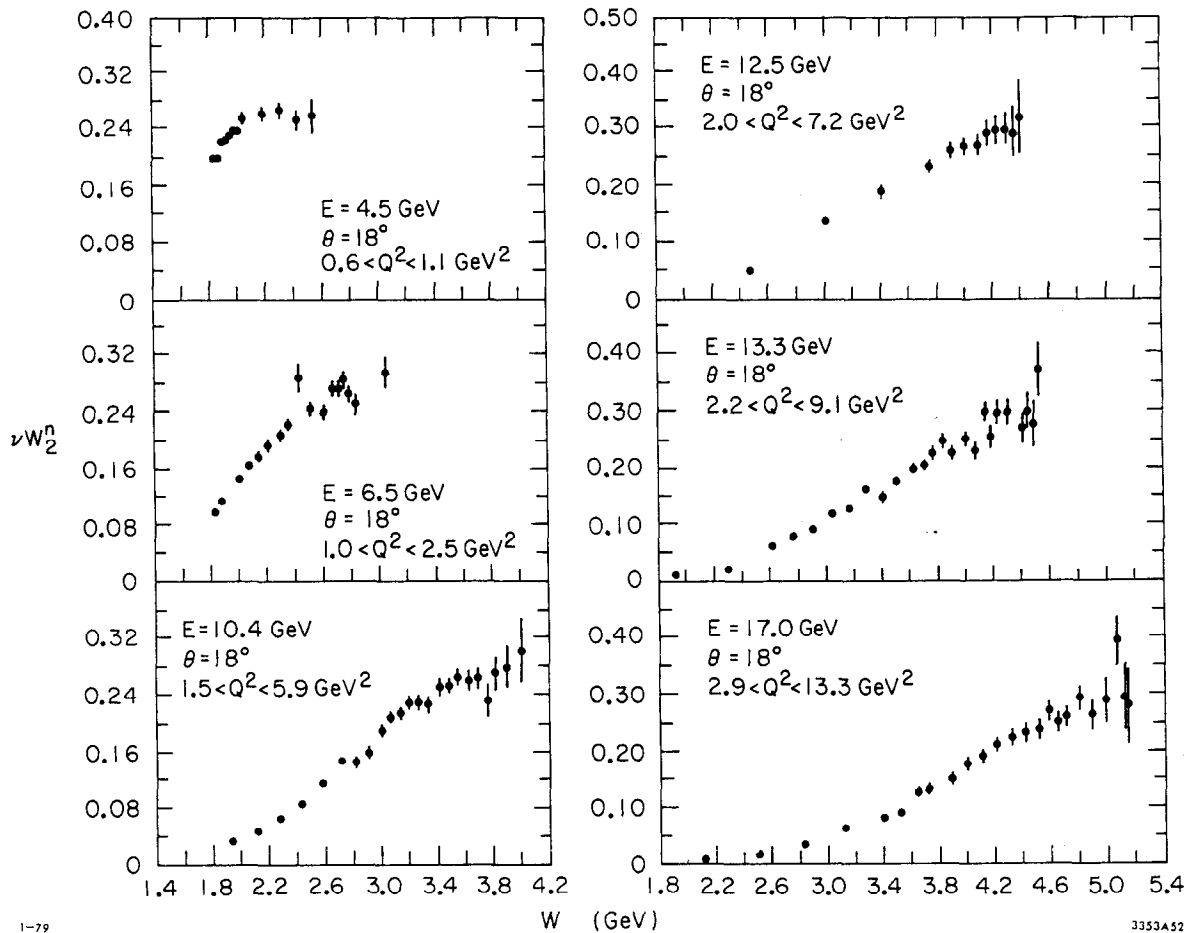


Fig. 21. The quantity νW_2^n extracted from inelastic $e - p$ and $e - d$ cross sections measured at 18° in experiment A.

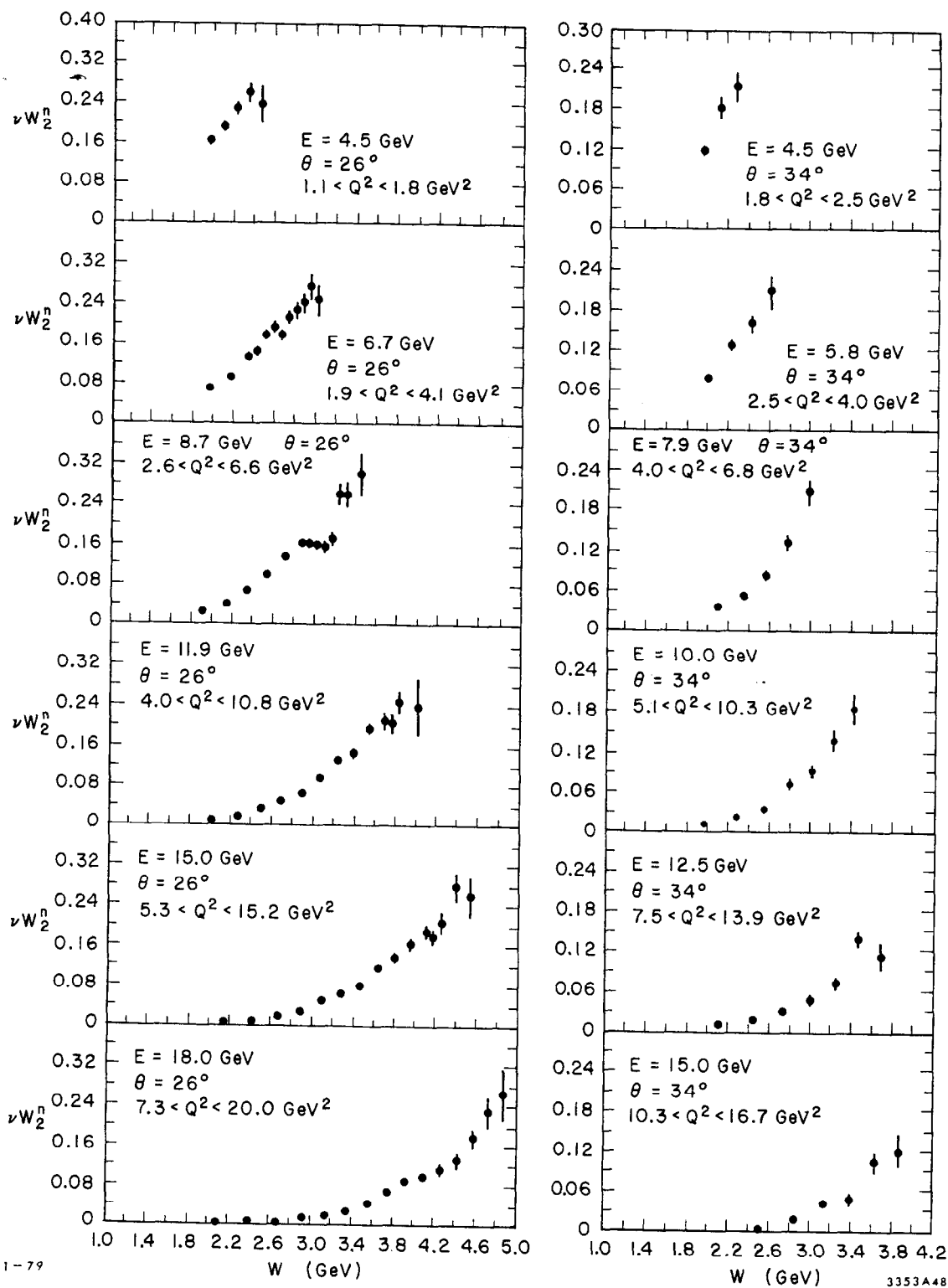
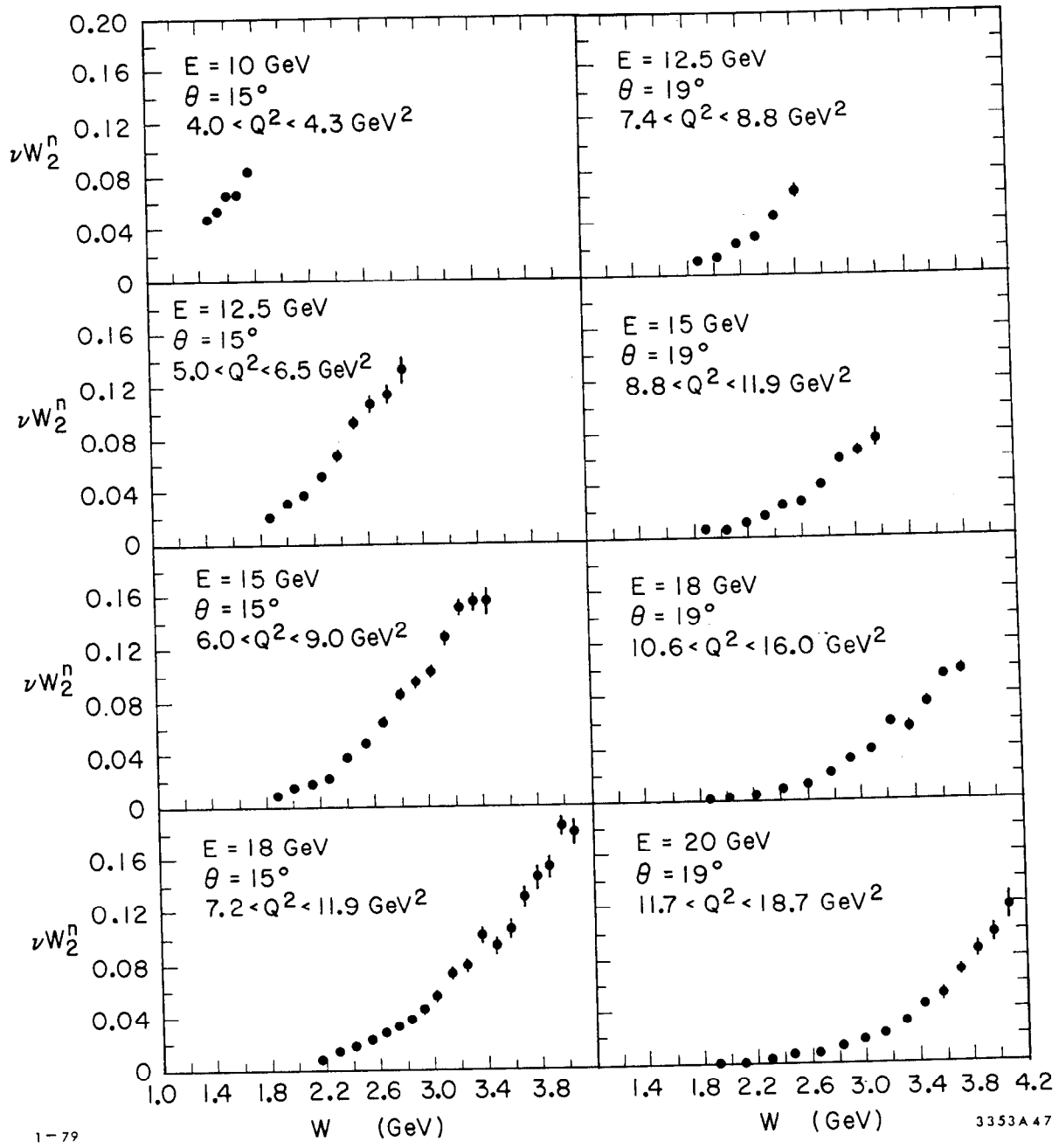


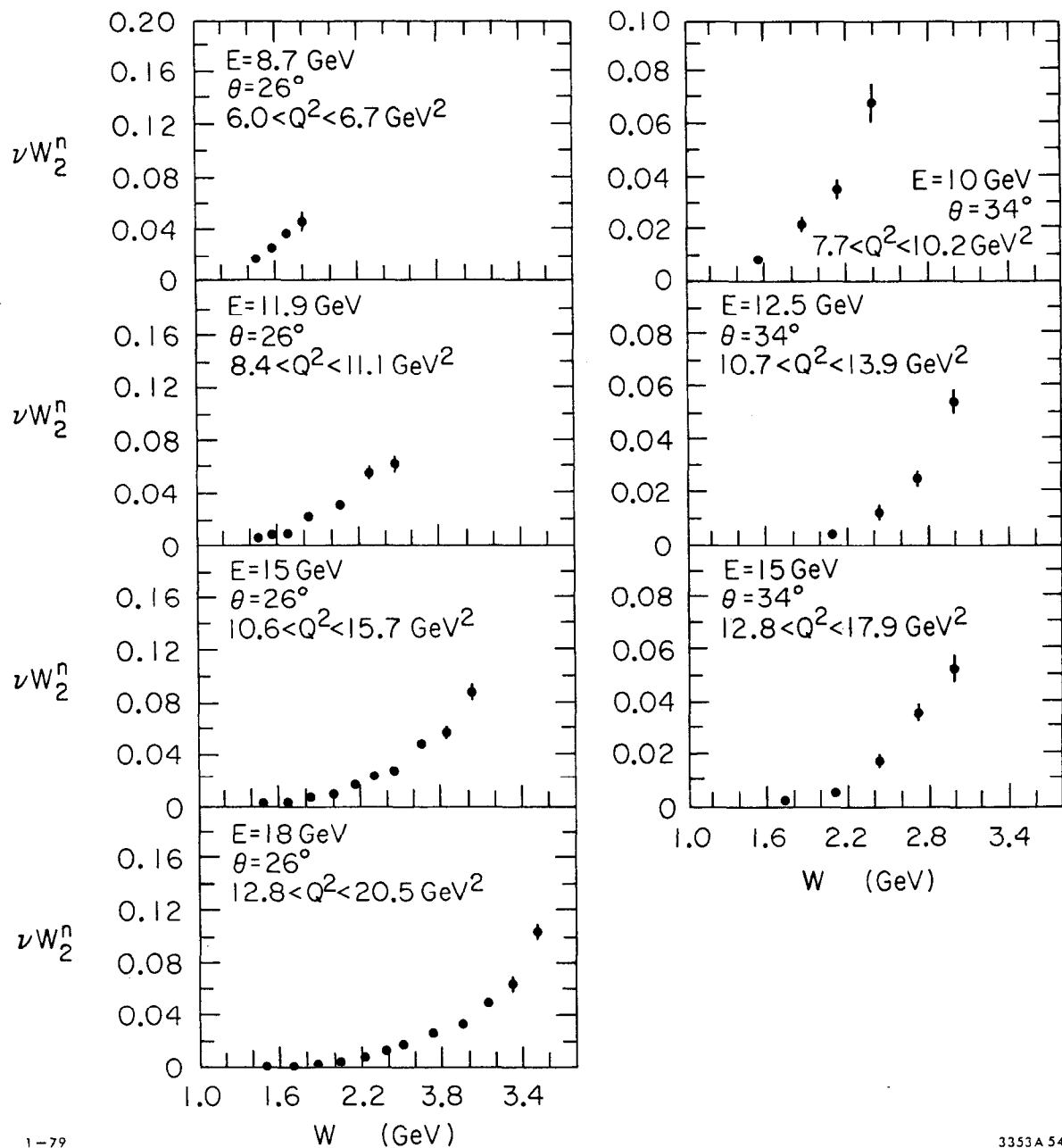
Fig. 22. The quantity νW_2^n extracted from inelastic $e - p$ and $e - d$ cross sections measured at 26° and 34° in Experiment A.



1-79

3353A47

Fig. 23. The quantity νW_2^n extracted from inelastic $e - p$ and $e - d$ cross sections measured at 15° and 19° in experiment B.



1-79

3353A 54

Fig. 24. The quantity νW_2^n extracted from inelastic $e - p$ and $e - d$ cross sections measured at 26° and 34° in experiment B.

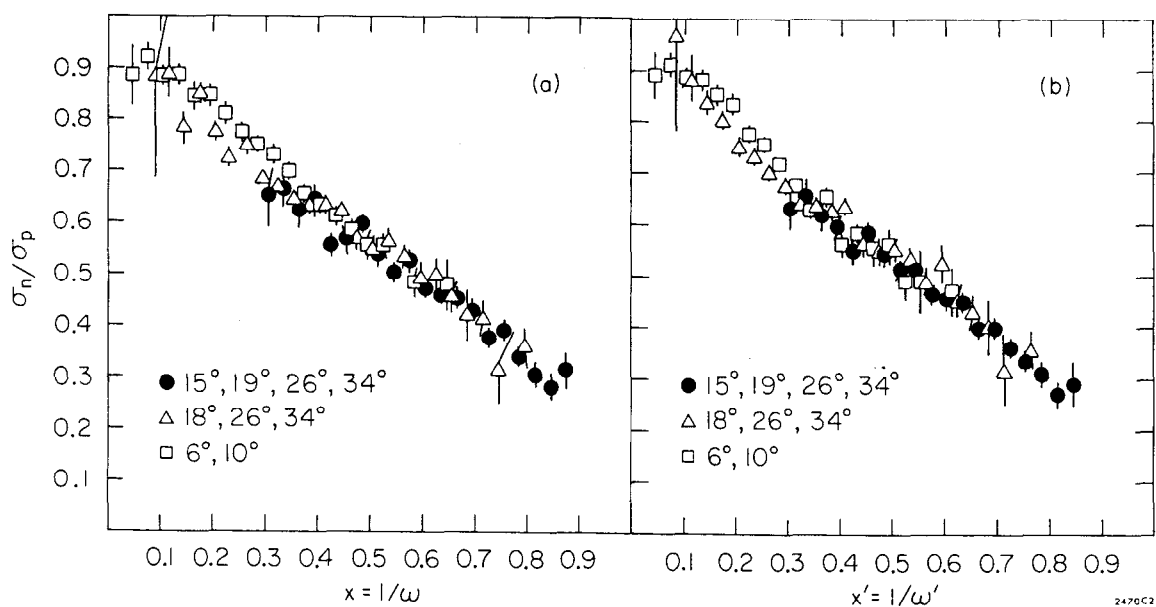


Fig. 25(a), (b). Values of σ_n/σ_p as determined from experiments A, B, and C as functions of x and x' respectively.

were combined separately in order to facilitate a comparison of the two sets of data. Individual values of σ_n and σ_p were normalized to the center of the bin in order to account for the small variation of σ_n/σ_p within a single bin. The σ_n/σ_p ratios are derived from σ_d/σ_p ratio measurements. The measured values for σ_d and σ_p are Poisson-distributed, but their ratio is not.^(64) Studies^(64) indicate that the quantity $\ln(1 + \sigma_n/\sigma_p)$ is approximately Gaussian-distributed. Therefore, the averaging involved forming the weighted geometrical mean of $(1 + \sigma_n/\sigma_p)$ for values in each x (or x') bin.

Only random errors (including counting statistics and also charge monitor, target density, and rate-dependent fluctuations) are shown in Figures (21 - 24). Most systematic errors in the cross sections (solid angle, E and E' calibration, monitor calibration, etc.) cancel in the ratio σ_n/σ_p . Of those which do not cancel, we estimate systematic uncertainties arising from five sources. Uncertainties in the deuteron elastic and quasi-elastic radiative tails arising from lack of knowledge of the neutron form factors at large Q^2 contribute a small error of about 0.002 to σ_n/σ_p . Uncertainties from the remaining four sources are listed separately in Table (x). The first column gives the experimental error due to the $\pm 1\%$ uncertainty in the ratio of the number of nuclei in the deuterium target to that in the hydrogen target. The other

three columns give errors due to uncertainties in the deuterium smearing corrections. The smearing and unsmearing corrections, which were calculated using the Hamada-Johnston⁴⁸ wave function, changed the uncorrected σ_n/σ_p ratios by multiplicative factors of 1.08, 1.07, 1.01, 0.91, 0.74, and 0.40 at x values of 0.31, 0.58, 0.67, 0.73, 0.79, and 0.88 respectively. The uncertainty quoted as "wave function" reflects the change in σ_n/σ_p when other reasonable deuteron wave functions⁽⁶⁵⁾ are used (see Appendix III). The uncertainty quoted as "off-shell" is taken to be the full effect of the off-mass-shell correction⁽⁶³⁾ in the smearing formalism (see Appendix III). This correction is such as to reduce σ_n/σ_p . The uncertainty quoted as "fit" reflects the change in σ_n/σ_p when different parametric functions are used to fit the neutron and proton structure functions which enter into the smearing and unsmearing integrals. The choice $R_n = R_p = 0.18$ was used in the process of obtaining the parametric representations of the structure functions. The extracted σ_n/σ_p ratios were insensitive to the kinematic dependence of R . In addition, Glauber corrections are known to be small⁽²⁰⁾. Other deuteron corrections cannot be estimated but are expected to be small (see Appendix II).

The results of the previous 6° and 10° measurements^(27,28)

are also shown in Figures (21 - 24). The data from the previous experiment were rebinned into small x and x' intervals ($\Delta x = 0.03$) as in the two experiments reported here.

V.E. Combined Cross Sections

The fine-mesh cross sections shown in Figures (9 - 16) were combined into the cross sections of Table (V) for use in the extraction of R and the structure functions. Only data with $W \geq 1.8$ GeV were used in this process, as data in the resonance region were not sufficiently smooth to permit this averaging. For the proton and deuteron data as many as eight adjacent fine-mesh cross sections $\sigma_i(E, \theta, E'_i) \pm \delta\sigma_i(E, \theta, E'_i)$ were combined to yield an average cross section $\bar{\sigma}(E, \theta, E') \pm \delta\sigma(E, \theta, E')$ at average E' according to the formula

$$\bar{\sigma}(E, \theta, E') = \sigma^f(E, \theta, E') r$$

$$\delta\sigma(E, \theta, E') = \sigma^f(E, \theta, E') \delta r$$

where

$$r = \frac{\sum_i \frac{r_i^2}{(\delta r_i)^2}}{\sum_i \frac{r_i}{(\delta r_i)^2}} \quad \delta r = \left| \frac{\sum_i \frac{r_i}{(\delta r_i)^2}}{r} \right|^{1/2} \quad (V.6)$$

using

$$r_i = \sigma_i(E, \theta, E'_i) / \sigma^f(E, \theta, E'_i)$$

$$\text{and} \quad \delta r_i = \delta\sigma_i(E, \theta, E'_i) / \sigma^f(E, \theta, E'_i)$$

Here σ^f is the appropriate cross section determined using the

global fit to νW_2 with the assumption $R_p = R_d = R_n = 0.18$ in equation (I.5).

Only the errors from counting statistics (see section V.B) were used in this averaging procedure. As the measurements of the cross sections were then Poisson-distributed, especially for low statistics runs, the averaging procedure used (equation V.6) was the Poisson-arithmetic average, according to the maximum likelihood method. As mentioned in section V.B, the random error from equipment fluctuations was added in quadrature to this average error from counting statistics to yield the values of $\delta\sigma$ given in Table (V). Where the cross section had already been averaged over the entire spectrometer acceptance before the radiative corrections, no combination had to be done, and only the random error from equipment fluctuations needed to be added in quadrature.

The combined neutron cross sections were obtained in a slightly different manner. Because σ_p , σ_d , and σ_{ps} are Poisson-distributed but $(\sigma_d - \sigma_{ps})$ is not, we could not average $(\sigma_d - \sigma_{ps})$ and then multiply by the average neutron smearing correction to get the average σ_n (see equation (V.4)). Therefore, we formed the neutron smearing correction $s_n = \sigma_n / (\sigma_d - \sigma_{ps})$ for each fine mesh data point, combined the products $\sigma_n \sigma_d$ and $\sigma_n \sigma_{ps}$ according to the prescription of equations (V.6), and then took the difference of the two products to get the combined value of σ_n . The random errors from equipment fluctuations for both the proton and deuteron were added in quadrature to the average error from counting statistics to yield the values of $\delta\sigma_{(E,\theta,E')}$ given in Table (V).

V.F. Normalizations

Although the inelastic e-p and e-d cross sections were measured with much the same apparatus in the two experiments, the use of different targets and differences in the analysis procedures permitted a relative normalization difference between the two experiments. As such normalization differences could have seriously influenced the results for $R = \sigma_L/\sigma_T$, an estimate of them was deemed essential. Two methods were used to estimate the relative normalization factor N_{AB} of experiment B to experiment A, and both gave results consistent with $N_{AB}^p = N_{AB}^d = 1.010$.

In the first method, the inelastic e-p and e-d cross sections measured at 26° and 34° in experiment B were compared with those measured at nearly identical energies and angles in experiment A. At 26° , we had to compare fine-mesh cross sections from experiment B with cross sections that had been averaged over the entire spectrometer acceptance in experiment A. Up to eight adjacent fine-mesh cross sections were combined in the manner of equation (V.6) to yield a single cross section for values of E and E' close to those quoted in experiment A. The normalization factor of experiment B to experiment A was then taken, at each common kinematic point, to be

$$N_{AB}(E_A, E'_A, \theta_A) = \left(\frac{\sigma_A(E_A, E'_A, \theta_A)}{\sigma_B(E_B, E'_B, \theta_B)} \right) \left(\frac{\sigma^f(E_B, E'_B, \theta_B)}{\sigma^f(E_A, E'_A, \theta_B)} \right) \quad (V.7)$$

Table XI. Normalization factors

θ (deg)	E (GeV)	N_{AB}^p	N_{AB}^d	\bar{N}_{AB}
26	8.7	0.985 ± 0.031	1.028 ± 0.024	1.012 ± 0.019
26	11.9	1.043 ± 0.022	1.027 ± 0.017	1.033 ± 0.013
26	15.0	1.009 ± 0.020	1.010 ± 0.014	1.010 ± 0.011
26	18.0	1.015 ± 0.021	1.005 ± 0.015	1.008 ± 0.012
26	all	1.017 ± 0.012	1.015 ± 0.008	1.015 ± 0.006
34	10.0	0.960 ± 0.041	0.953 ± 0.026	0.955 ± 0.022
34	12.5	0.965 ± 0.045	0.994 ± 0.029	0.985 ± 0.024
34	15.0	1.011 ± 0.043	1.028 ± 0.030	1.022 ± 0.025
34	all	0.979 ± 0.025	0.989 ± 0.016	0.984 ± 0.014
all	all	1.010 ± 0.010	1.010 ± 0.007	1.010 ± 0.006

where σ^f is defined as before, and equation (V.7) applies for proton and deuteron cross sections. Use of σ^f in equation (V.7) eliminates the effects of slight differences in E , E' , and θ settings between the two experiments. Averages of these normalization factors for each common value of incident energy and angle are presented in Table (XI). Only cross sections for $W \geq 1.8$ GeV were used in calculating these factors. The normalization factors for the proton and deuteron were always within one standard deviation of their average. If we average over the entire sample of 26° and 34° data, we find $N_{AB}^p/N_{AB}^d = 1.001 \pm 0.013$; hereafter, we take $N_{AB}^p = N_{AB}^d$. The average 34° normalization factors for both the proton and deuteron were more than one standard deviation from the overall average. These differences could be traced only to a few abnormally low cross sections in experiment A, however, and were not the general trend of the data. Separate normalization factors for the 26° and 34° data were not clearly warranted. Consequently, the relative normalization of experiment B to experiment A was taken to be the average of the 26° and 34° results, or $N_{AB}^p = 1.010 \pm 0.010$ for the proton and $N_{AB}^d = 1.010 \pm 0.007$ for the deuteron cross sections. These factors have been included in the cross sections of Table (V).

A second estimate of N_{AB} was obtained from a comparison of elastic e-p cross sections measured in the two experiments.

Differential elastic e-p cross sections from the two experiments were radiatively corrected according to the method of Tsai. (45)

They were then divided by the dipole cross section $(\frac{d\sigma}{d\Omega})_{\text{dip}}$, which was calculated by assuming form factor scaling and the dipole form factor, $G_{Ep} = G_{Mp}/\mu_p = (1 + Q^2/0.71)^{-2}$ in the Rosen-

bluth equation. (51) Ratios $r(Q^2)$ of measured to dipole differential cross sections are presented in Figure (26) for the two experiments along with values of $r(Q^2)$ measured⁽²⁷⁾ in experiment C. A fourth order polynomial fit $r_A^f(Q^2)$ to the values of $r_A(Q^2)$ was compared to the three values of $r_B(Q^2)$ measured at 15° and one value measured at 19° in experiment B. The average of $N_{AB}^p = r_A^f(Q^2)/r_B(Q^2)$ over all four measurements was $N_{AB}^p = 1.012 \pm 0.010$, while the average at 15° only was $N_{AB}^p = 1.002 \pm 0.012$. Both numbers are consistent with the normalization factor $N_{AB}^p = N_{AB}^d = 1.010$ derived from the 26° and 34° inelastic comparisons.

A similar method⁽²⁶⁾ was used to compute the normalization factor N_{AC} for experiment C. Only the elastic e-p cross sections measured at 10° were used, as the systematic uncertainty in the scattering angle^(27, 66) was too large at 6° to permit a reliable comparison. The polynomial fit $r_A^f(Q^2)$ was compared to seven values of $r_C(Q^2)$ shown in Figure (26), resulting in an average normalization factor $N_{AC}^p = 1.019 \pm 0.011$, where the quoted error is purely random. Systematic uncertainties in N_{AC}^p arise from uncertainties that affect the elastic cross sections in a manner different from the inelastic cross sections. These include uncertainties in E and $\theta (\pm 0.8\%)$,

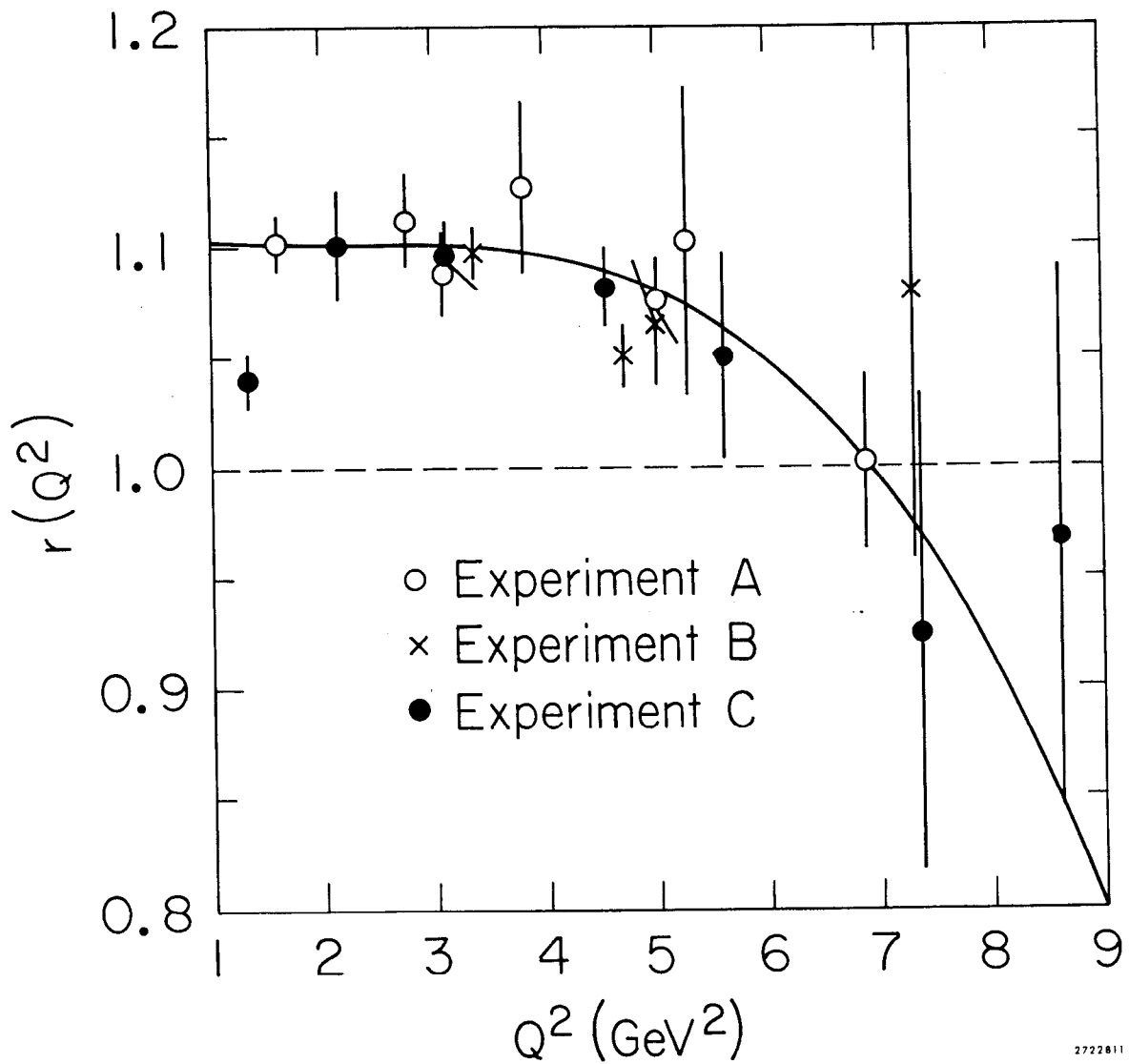


Fig. 26. Ratios, $r(Q^2)$, of the elastic $e - p$ cross sections measured in experiments A, B, and C to elastic cross sections calculated using the dipole form factor in the Rosenbluth equation.

approximations in the radiative corrections ($\pm 0.7\%$), the assumption of form factor scaling ($\pm 0.5\%$), and differences between the two experiments ($\pm 0.6\%$), in the method of binning the data to calculate $(\frac{d\sigma}{d\Omega})_{\text{elast}}$. Added in quadrature to the random error, these effects led to the result $N_{AC}^p = 1.019 \pm 0.017$. A determination of the normalization factor N_{AC}^d for the small angle inelastic e-d cross sections from quasi-elastic e-d cross sections was judged unfeasible due to uncertainties arising both from inelastic background subtractions and from corrections for deuteron binding effects. Therefore, the proton normalization factor was used for the deuteron cross sections of experiment C, $N_{AC}^d = 1.019 \pm 0.024$, with an additional systematic uncertainty of ± 0.021 added in quadrature to the 0.011 error to account for uncertainties in target lengths and densities.